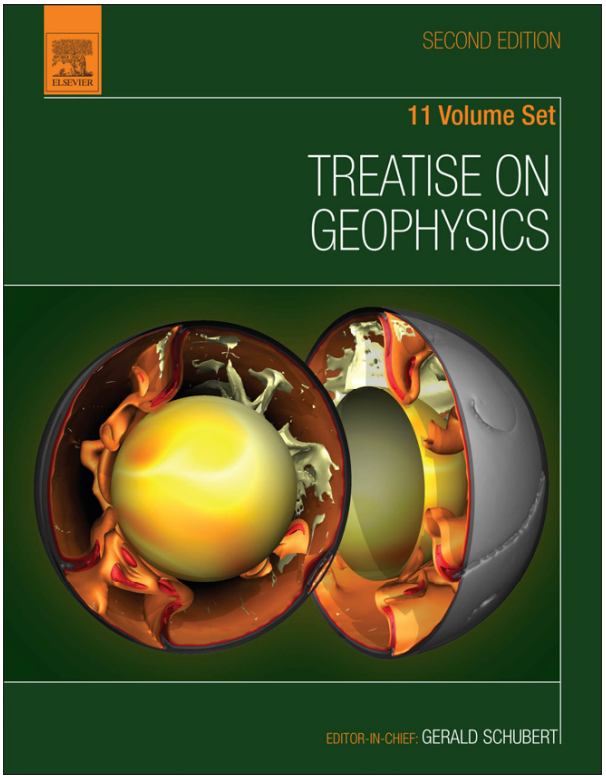

Manga M., and Wang C.-Y Earthquake Hydrology. In: Gerald Schubert (editor-in-chief) Treatise on Geophysics, 2nd edition, Vol 4. Oxford: Elsevier; 2015. p. 305-328.

4.12 Earthquake Hydrology

M Manga and C-Y Wang, University of California, Berkeley, CA, USA

4.12.1 Introduction

For thousands of years, changes in the amount, direction, and rate of water flow in streams and in fluid pressure in the subsurface have been documented following large earthquakes. Examples include the formation of new springs, disappearance of previously active springs, increased discharge in streams by up to an order of magnitude that persists for weeks or even months, fluctuations in water levels in wells by several meters, and permanent changes in water levels in wells coincident with earthquakes located thousands of kilometers away. Such observations, although often simply assigned to the category of curious phenomena, provide unique insight into hydrogeologic processes and, in particular, their correlation with tectonic processes at spatial and temporal scales that could otherwise not be studied.

Hydrologic responses are not unexpected: Earthquakes cause strain, and strain changes fluid pressure and alters hydrogeologic properties such as permeability, which controls the rate of fluid flow. What is more surprising about many hydrologic responses, however, is their large amplitude and the great distances over which they occur.

This chapter is divided into two main parts. First, we describe the processes by which fluid pressure and hydrologic properties can change following an earthquake. Next, we review hydrologic phenomena attributed to earthquakes and summarize our current state of understanding about the processes that cause these phenomena. We then conclude with a brief discussion of possible hydrologic precursors to earthquakes.

4.12.2 Hydrologic Response to Stress

Earthquakes change the static stress (i.e., the offset of the fault generates a static change in stress in the crust) and also cause dynamic stresses (from the seismic waves). Both stresses increase as the seismic moment of the earthquake, but they decay very differently with distance r. Static stresses decrease as $1/r^3$. By comparison, dynamic stresses, which are proportional to the seismic wave amplitude, decrease more gradually. A standard empirical relationship between surface wave amplitude and magnitude has dynamic stress decreasing as $1/r^{1.66}$ (e.g., Lay and Wallace, 1995). Other factors such as directivity, radiation pattern, and crustal structure will also influence the amplitude of shaking. However, the significant difference in the dependence on distance is a robust feature distinguishing static and dynamic stresses.

Table 1, reproduced from Manga and Brodsky (2006), lists and compares the magnitude of earthquake stresses with other external stresses of hydrologic interest. Both static and dynamic stresses may be significant in the near field and intermediate field (within up to a few fault lengths), but only dynamic

Treatise on Geophysics, 2nd edition, (2015), vol. 4, pp. 305-328

Table 1 Amplitude and period of stress changes of earthquakes compared with other sources of stress

	Stress (MPa)			*Period*
Solid earth tides	10^{-3}			12 h
Ocean tides	10^{-2}			12 h
Hydrologic loading	$10^{-3}-10^{-1}$			Days–years
Glacier loading	$10^{1}-10^{2}$			10^{3} years
Epicentral distance	10^{2} km	10^{3} km	10^{4} km	
Static stress changes, M8	10^{-1}	10^{-4}	10^{-7}	NA
Dynamic stress changes, M8	3	0.06	0.001	20 s

Adapted from Manga M and Brodsky EE (2006) Seismic triggering of eruptions in the far field: Volcanoes and geysers. *Annual Review of Earth and Planetary Sciences* 34: 263–291.

stresses are larger than tidal stress in the far field (many fault lengths away).

4.12.2.1 Effect of Static Stress

4.12.2.1.1 Poroelastic flow and deformation

In response to stresses, porous solids deform, the pressure of fluids within pores changes, and pore fluids can flow. The basic theory of poroelasticity, first developed by Biot (1941, 1956a,b), describes the coupling between changes in stress σ, strain ϵ, pore pressure p, and the material properties that relate these three variables. A complete discussion and derivation of the theory, even its simplest forms, is beyond the scope of this chapter, but several key relationships are useful for understanding the hydrologic response to earthquakes and interpreting observations. Wang's (2000) text on linear poroelasticity and review papers by Rice and Cleary (1976), Roeloffs (1996), and Neuzil (2003) provide thorough and pedagogical reviews.

Consider an isothermal, linear, isotropic poroelastic material subjected to a stress σ_{ij}. The material will respond by deforming with the total strain ϵ_{ij}, given by

$$\epsilon_{ij}=\frac{1}{2G}\left[\sigma_{ij}-\frac{v}{1+v}\sigma_{kk}\delta_{ij}\right]+\frac{\alpha}{3K}p\delta_{ij} \qquad [1]$$

where G is the shear modulus, K is the bulk modulus, v is the Poisson ratio, and α is the Biot–Willis coefficient, which is the ratio of the increment in fluid content to the volumetric strain at constant pore pressure. The increment in fluid content, denoted ψ, is the change in fluid mass per unit volume divided by the density of the fluid at the reference state and is given by

$$\psi=\frac{\alpha}{3K}\sigma_{kk}+\frac{\alpha}{KB}p \qquad [2]$$

where B is called Skempton's coefficient and has a value between 0 and 1, with 'hard rocks' such as sandstone and granite having values between about 0.5 and 0.9 and unconsolidated materials having a value close to 1. The variable B is related to the porosity ϕ and to the compressibilities of the pore fluid, solid grains, and saturated rock. The sign convention is chosen so that negative σ_{kk} indicates compression.

First, we consider the so-called 'undrained' limit in which there is no flow of pore fluid, that is, $\psi=0$ (the opposite extreme, termed 'drained,' corresponds to the limit in which there is no change in fluid pressure, i.e., $p=0$). The change in pore pressure p caused by a change in mean stress σ_{kk} can be found from eqn [2]:

$$p=-\frac{B}{3}\sigma_{kk} \qquad [3]$$

Equation [3] can be expressed in terms of the volumetric strain ϵ_{kk} using constitutive relationship [1] and physical relationship [2]:

$$p=-\frac{B}{3}\sigma_{kk}=-BK_u\epsilon_{kk}=-\frac{2GB}{3}\frac{1+v_u}{1-2v_u}\epsilon_{kk} \qquad [4]$$

where the subscript u indicates a value under undrained conditions. Shear modulus G should have the same value in drained and undrained conditions for a linear poroelastic material.

If there are gradients of fluid pressure, there will be a flux of fluid $\mathbf{q}$ (volume/area per unit time) governed by Darcy's equation

$$\mathbf{q}=-\frac{k}{\mu}\nabla p \qquad [5]$$

where the pressure p is the excess pressure, that is, the pressure difference from hydrostatic, k is the permeability, and μ is the fluid viscosity. p, as defined, is equivalent to the hydraulic head multiplied by ρg, where ρ is the density of the fluid and g the gravitational acceleration. Darcy's equation, coupled with the continuity equation governing conservation of mass, if the permeability k and μ are constant, leads to pore pressure being governed by an inhomogeneous diffusion equation

$$\frac{\alpha}{KB}\left[\frac{B}{3}\frac{\partial\sigma_{kk}}{\partial t}+\frac{\partial p}{\partial t}\right]=\frac{k}{\mu}\nabla^2 p \qquad [6]$$

The term involving the time derivative of stress couples the mechanical deformation and the fluid flow. The time derivative of stress will not appear in the case of uniaxial strain and constant vertical stress, both reasonable approximations for near-surface aquifers (but not rigorously correct if there is two- or three-dimensional flow), and can be neglected for very compressible fluids such as gases (Wang, 2000). In these cases, the evolution of fluid pressure resulting from flow is uncoupled from that for the stress and can be solved independently. Equation [6] then reduces to the form commonly used to model groundwater flow:

$$S\frac{\partial p}{\partial t}=\frac{k\rho g}{\mu}\nabla^2 p \quad \text{or} \quad \frac{\partial p}{\partial t}=D\nabla^2 p \qquad [7]$$

where S is standard hydrogeologic specific storage and is equal to volume of water released per unit change in head while maintaining no lateral strain and constant vertical stress and D is called the hydraulic diffusivity.

Assuming eqn [7] is a good approximation, the timescale τ for changes in pore pressure to diffuse or relax can be calculated by $\tau\sim L^2/D$, where L is the length scale over which the pressure diffuses. Typical values of D are 10^{-10}–$10^{4}\,\mathrm{m^2\,s^{-1}}$, with small values characterizing low-permeability rocks (e.g., shale) and large values characterizing coarse, unconsolidated sediments or highly permeable rock (e.g., gravel and karst, respectively). A value of $10^{0}\,\mathrm{m^2\,s^{-1}}$ would be typical of

sandstone aquifers. For a 100 m thick layer, then, pore pressure changes will diffuse on timescales that range from minutes to many decades and with a timescale of hours for a sandstone aquifer.

We will see, when we examine hydrologic observations, that many of the most dramatic hydrologic phenomena mentioned in the introduction, and in particular those that involve water discharge at the Earth's surface, cannot be explained by traditional linear poroelasticity theory. The reason is quite straightforward. Consider the case in which a stress change σ_{kk} causes an undrained pressure change p given by eqn [3]. For a (very large) static stress change of 1 MPa (see **Table 1**), eqn [3] implies pressure changes of 0.1–0.3 MPa. This would cause a 10–30 m change in water level in a well. To bring the pore pressure back to its original value requires the removal of an increment of fluid content

$$\psi = \frac{3(v_u - v)}{2GB(1+v)(1+v_u)}\sigma_{kk} \qquad [8]$$

Using values for Berea sandstone (Wang, 2000) of $v = 0.17$, $v_u = 0.33$, $G = 5.6$ GPa, and $B = 0.75$, we obtain $\psi = 3.5 \times 10^{-5}$. For a 100 m thick aquifer with porosity $\phi = 0.4$, this is equivalent to about 1 mm of water per unit area discharged at the surface – an amount that is small compared with that needed to explain the excess discharge in streams following large earthquakes (see Table 1 in Manga, 2001).

Equations [1]–[3] apply for linear, isotropic porous materials. In this limit, shear stresses cause no change in pore pressure. In natural rocks, however, shear stresses can induce changes in pore pressure because of anisotropy or the nonlinear elastic behavior of rocks (e.g., Hamiel et al., 2005).

4.12.2.1.2 Permanent deformation

At shear strains from 10^{-4} to 10^{-3}, brittle rocks, sediments, and soils show permanent deformation. At even greater shear strains ($\sim 10^{-2}$), failure occurs. The changes in porosity of sediments and soils during permanent deformation may be many orders of magnitude greater than that during elastic deformation. Thus, under undrained conditions, permanent deformation can be associated with significant changes in pore pressure and groundwater flow.

During permanent deformation, the cohesion among the grains of sediments and soils is disrupted and the grains tend to move to reach a new state of equilibrium. The basic characteristics of deformation, however, depend on the consolidation state of sediments and soils. For loose deposits, shear deformation causes grains to move into preexisting pores. This reduces the original porosity and thus the volume of sediments (soils) decreases – a process commonly known as consolidation. Shear deformation of dense deposits, in contrast, will cause sediment grains to roll over each other and, in so doing, create new porosity; thus, the volume of sediments (soils) increases – a process commonly known as dilatancy. In both cases, a critical state is eventually reached in undrained deformation, beyond which porosity no longer changes with continued shearing.

The deformation behavior of brittle rocks is distinctly different from that of sediments and soils, leading to different predictions for the hydrologic and seismic consequences under applied stresses. Laboratory measurements show that beyond the elastic limit, shearing of consolidated rocks causes microcracks to open and the volume of rock to increase – that is, they become dilatant (e.g., Brace et al., 1966). At still higher deviatoric stresses, microcracks may coalesce and localize into a shear zone, leading to eventual rupture (Lockner and Beeler, 2002). Repeated rupturing of the brittle crust along a fault zone can produce pulverized gouge material with significant porosity. Geologic investigations of exhumed fault zones in California (e.g., Chester et al., 1993, 2004) and in Japan (Forster et al., 2003; Wibberley and Shimamoto, 2003) and studies of drilled cores from fault zones (e.g., Ohtani et al., 2001; Zoback et al., 2010) have demonstrated that some fault zones are composed of fluid-saturated, porous fault gouge several hundred meters thick. Attempts to image the structure of fault zones by using conventional seismic reflection and refraction methods (e. g., Thurber et al., 1997) suffered from not having high enough station and source densities to resolve deep fault zone structures on the scale of hundreds of meters (Mizuno, 2003). However, seismic imaging of the fault zone structures with fault zone trapped waves (e.g., Li and Malin, 2008; Li et al., 2000; Mizuno and Kuwahara, 2008) and high-frequency body waves (Li and Zhu, 2007) has delineated a 100–250 m wide gouge zone along active faults in California (Li and Zhu, 2007; Li et al., 2000) and in Japan (e.g., Mizuno, 2003) in which the seismic velocities are reduced by 30–50% from the wall-rock velocities. Direct drilling of the San Andreas Fault zone to a depth of ~3 km near Parkfield, CA, also revealed a process zone 250 m in width, in which the seismic velocities are 20–30% below the wall-rock velocities (Zoback et al., 2010).

Using high-resolution electromagnetic imaging, Unsworth et al. (2000) showed that the San Andreas Fault zone contains a wedge of low-resistivity material extending to several kilometers in depth; they further suggested a range of saturated porosity to account for the observed electrical resistivity. Using experimentally measured seismic velocity and electrical conductivity of fault gouge at elevated pressures to interpret the then-available seismic velocity and electrical resistivity of the San Andreas Fault zone in Central California, Wang (1984) suggested that the fault zone may consist of saturated fault gouge. Inverting the gravity anomaly across the San Andreas Fault zone in Central California and constraining the inversion by using existing seismic reflection profiles, Wang et al. (1986) further showed that the fault zone may be characterized by relatively low density with a corresponding porosity greater than 10% extending to seismogenic depths.

That fault zones may be porous and saturated at seismogenic depths has important implications for a host of issues related to the dynamics of faulting (e.g., Andrew, 2003; Brodsky and Kanamori, 2001; Lachenbruch, 1980; Mase and Smith, 1987; Sibson, 1973; Sleep and Blanpied, 1992; Wibberley and Shimamoto, 2005), the strength (or weakness) of faults (e.g., Lachenbruch and Sass, 1977; Mount and Suppe, 1987; Rice, 1992; Zoback et al., 1987), and the forces that move lithospheric plates (e.g., Bird, 1978). To obtain direct information on the pore pressure in fault zones, drilling into active faults has been attempted around the world in the past decades (San Andreas Fault Observatory at Depth, SAFOD, near Parkfield in Central California (Zoback et al., 2010), the

Nojima Fault Zone Probe in Japan, the Chelungpu Fault Drilling Project in Taiwan (see Brodsky et al., 2010, for a summary of the Nojima and Chelungpu projects), and an ongoing project to drill into the New Zealand South Island Alpine Fault, Gorman, 2011). The SAFOD drilling project is the best documented and has provided invaluable information about the internal structure of the San Andreas Fault zone (e.g., Zoback et al., 2010). At a depth of ~2.7 km, the SAFOD drilling encountered three actively slipping, clay-rich gouge zones, each 23 m wide. Three observations made during drilling led Zoback et al. (2010) to conclude that there was no evidence of high pore pressure in the fault cores: (1) no excess influx of aqueous formation fluids from the fault zone into the borehole, (2) no excess inflow of formation gas into the borehole, and (3) a near-constant V_p/V_s ratio across the fault zone (where V_p and V_s are the velocities of the compressional and the shear seismic waves, respectively). However, quantitative simulation of the expected flow of aqueous fluids and gases into the well during drilling and the V_p/V_s ratios normal to the drilling direction (Wang, 2011), based on laboratory data for the permeability of fault zone material (Chu et al., 1981; Marone et al., 2010; Morrow et al., 1984; Rathbun et al., 2010) and the seismic wave velocities in layered rocks (Lo et al., 1986), showed that the time duration during drilling may not be long enough to detect any flow of aqueous fluids and gases into the well and that the V_p/V_s ratio measured may not be sensitive enough to determine whether high pore pressure does exist in the fault zone. Thus, long-term monitoring of pore pressure may be required to provide definite knowledge of whether high pore pressure does or does not exist in fault zones.

4.12.2.2 Effect of Dynamic Strain

4.12.2.2.1 Poroelastic deformation and fluid flow

Seismic waves cause spatial variations in strain and hence spatial variations in pore pressure. The resulting pore pressure gradients cause fluid flow. Seismic wave speeds in saturated rocks will thus differ from those in unsaturated rocks and will be frequency-dependent. As the fluid moves, energy is also dissipated by the fluid flow, which in turn is governed by the permeability of the porous material, the geometry of the pores, and the viscosity of the fluid. This contributes to seismic attenuation. Wave speed and attenuation can be calculated theoretically as a function of frequency for porous materials with different pore structures by solving the poroelastic equations coupled with Darcy's equation for fluid flow at the macroscopic scale. As frequency increases, pore scale (or 'squirt') flows become more important (e.g., Mavko et al., 1998). These ideas were first quantified in a series of papers by Biot (e.g., Biot, 1941, 1956a,b, 1962) and extended by many authors since, for example, by accounting for squirt flows (e.g., Dvorkin et al., 1994). Additional important extensions to actual geologic settings include accounting for heterogeneity with dual-porosity models (e.g., Berryman and Wang, 2000) or fractal geometries (e.g., Masson and Pride, 2006) and partial or multiphase saturation (e.g., Pride et al., 2004).

Changes in pore pressure and stress also change fracture and pore geometry, which in turn alters wave speeds and anisotropy. The frequency dependence of attenuation and wave speeds also depends on hydrogeologic properties such permeability and the nature of permeability heterogeneity. The relationship between seismic properties, hydrogeologic properties, and fluid pressure involves so many parameters that inferring particular properties of the subsurface from seismic measurements is challenging. However, measurements of seismic attenuation, seismic anisotropy, and wave speeds can be used as a noninvasive probe to monitor changes in the subsurface (e.g., Liu et al., 2004).

4.12.2.2.2 Permanent deformation

The dynamic deformation of sediments and soils, in contrast to the static deformation, is affected by inertial forces that depend on loading rates and number of loading cycles. An often-used measure of the total amount of seismic energy imparted to an engineered structure is the Arias intensity, which is proportional to the square of acceleration (Arias, 1970; Jennings, 2003). Therefore, even if the magnitude of stresses is small, inertial forces may significantly affect deformation at high frequencies. For this reason, it is necessary in earthquake engineering to examine the dynamic deformation of sediments and soils for dynamic strains as small as 10^{-6}. Permanent volumetric deformation, however, does not occur until the magnitude of shear strain reaches some threshold. Dobry (1989) summarized undrained experimental results in which excess pore pressure developed during the application of ten cycles of sinusoidal loads. He showed that, for different sands with a wide range of dry densities subjected to a wide range of effective confining pressures, pore pressure did not increase until the cyclic shear strain amplitude was increased to 10^{-4}. The increase in pore pressure indicates a decrease in pore volume, and hence consolidation. It is interesting to note that the strain threshold is comparable in magnitude to that for permanent deformation to occur in static deformation (**Section 4.12.2.1**).

The number of loading cycles during dynamic loading is another important factor in determining the mechanical responses of sediments and soils. Results of laboratory experiments show that during cyclic loading at constant strain amplitude, pore pressure in sediments and soils increases with the number of loading cycles. At decreasing strain amplitudes, a greater number of loading cycles is required to build up excess pore pressure to a given magnitude (Ishihara, 1996). During large earthquakes, about 10–20 cycles of major ground shaking occur, though the amplitude of each cycle will vary.

4.12.2.2.3 Liquefaction

When pore pressures approach the overburden pressure, soils lose their rigidity and become fluidlike – a phenomenon widely known as liquefaction (Seed and Lee, 1966; Terzaghi et al., 1996), which is a major source of seismic hazard for engineered structures. Liquefied sediments and soils in the subsurface are associated with substantial pore pressure, as indicated by the height of the smear on the wall in **Figure 1**, left by ejected sands during the 1999 M7.5 Chi-Chi earthquake in Taiwan. Most liquefaction occurs near the ruptured fault, but a large number of examples of liquefaction have been documented at distances beyond the near field (Wang, 2007).

Field and laboratory studies show that the occurrence of liquefaction depends on many factors, such as earthquake magnitude, shaking duration, peak ground motion, depth to the groundwater table, basin structures, site effects, and

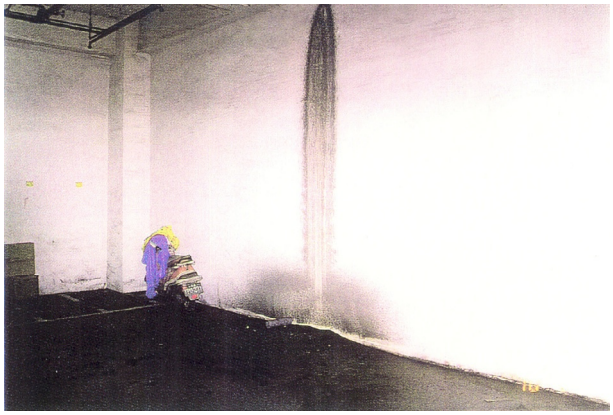

Figure 1 Smear of sediment left on a building wall created by ejected sand during the 1999 M7.5 Chi-Chi earthquake in Taiwan. Motorcycle at lower left shows scale. Reproduced from Su T-C, Chiang K-W, Lin S-J, Wang F-G, and Duann S-W (2000) Field reconnaissance and preliminary assessment of liquefaction in Yuan-Lin area. *Sino-Geotechnica* 77: 29–38.

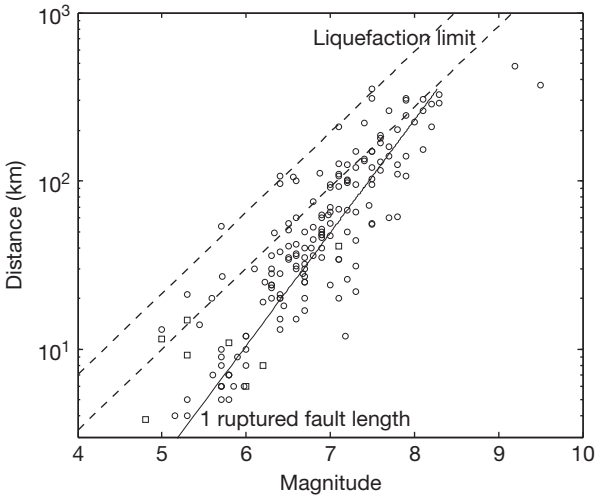

Figure 2 Relationship between earthquake magnitude (moment magnitude when known) and the distance between the earthquake epicenter and occurrence of liquefaction. Data shown with circles are from the compilation in Wang and Manga (2010a). Squares show data following the M7.1 2010 Darfield, New Zealand, earthquake and seven of its aftershocks (Simon Cox, GNS New Zealand, written communication) and responses to the M7.2 Fiordland, New Zealand, earthquake of 2003 (Hancox et al., 2003). For most of the New Zealand events, only the maximum distance for each earthquake is plotted. The dashed lines delineate an upper bound for the maximum distance over which shallow liquefaction has been observed and correspond to estimates of dissipated seismic energy density between 0.1 and 1 J m^{-3} (Wang, 2007). The solid line indicates one ruptured fault length based on the regression of Wells and Coppersmith (1994) and bounds the near field.

liquefaction susceptibility of sediments (e.g., Youd, 2003). Thus, the occurrence of liquefaction is difficult to predict on a theoretical basis, and empirical approaches are as a rule adopted in assessing the liquefaction potential of an area. Various ground penetration tests (e.g., Bardet, 2003) are routinely done during the geotechnical assessment of sites. On large scales, empirical relations between the magnitude of ground shaking and liquefaction (e.g., Wang et al., 2003) may be combined with numerical simulations of ground shaking during an earthquake (e.g., Stidham et al., 1999) to evaluate the regional liquefaction potential. Such applications, however, require extensive information about sediment properties and subsurface structures of the area of interest. In areas where such data are not available, a simpler approach may be applied to set some limits to the expected extent of liquefaction during potential earthquakes. Field observations show that, for earthquakes of a given magnitude M, the occurrence of liquefaction is confined within a particular distance from the earthquake epicenter, that is, the liquefaction limit $R_{\max}$ beyond which liquefaction is not expected (Ambraseys, 1988; Galli, 2000; Kuribayashi and Tatsuoka, 1975; Papadopoulos and Lefkopulos, 1993; Wang et al., 2005a; Wang, 2007). **Figure 2** shows a compilation of data for the occurrence of liquefaction and an empirical bound on the relationship between $R_{\max}$ and M (Wang, 2007); all data and references are tabulated in Wang and Manga (2010a) with additional data from the M7.1 2010 Darfield, New Zealand, earthquake and its aftershocks (Simon Cox, GNS, New Zealand, written communication) and responses to the M7.2 Fiordland, New Zealand, earthquake (Hancox et al., 2003). The empirical bounds correspond to estimates of dissipated seismic energy density e between 0.1 and 1 J m^{-3} (Wang and Manga, 2010b). e is defined as

$$e = \frac{1}{2}\sum_i \frac{\rho}{T_i}\int v_i(t)^2 \mathrm{d}t \qquad [9]$$

where the sum is taken over all modes of ground motion, ρ is density, and T_i and v_i are the period and velocity of the ith mode, respectively. Also shown for reference in **Figure 2** is the length of the ruptured fault as a function of M, based on the regression of Wells and Coppersmith (1994). While the data plotted in **Figure 2** neglect important features such as site effects and directivity, they do indicate that liquefaction occurs at distances beyond the near field (Wang, 2007). The liquefied sites near the liquefaction limit are likely to be those with the optimal conditions for liquefaction, that is, saturated soils with high liquefaction susceptibility or strong directivity effects. Liquefaction at closer distances may include sites with less optimal conditions that are exposed to greater seismic input.

Because liquefaction damages engineered structures, there has been a concerted research effort, both in the laboratory and in the field, to understand the processes of liquefaction and to predict its occurrences (for an overview of these efforts, see Bardet, 2003; National Research Council, 1985; Youd, 2003). In laboratory studies, sediment and soil samples are often obtained from the field and subjected to cyclic loading. At constant amplitude of deviatoric stress (stress minus the mean normal stress), deformation may be stable up to some number of cycles of shearing, but sudden onset of large shear deformation (onset of liquefaction) may occur if the cycles of shearing exceed some threshold number (e.g., National Research Council, 1985). The onset of liquefaction occurs once the effective stress (defined later in eqn [16]), which decreases with increasing pore pressure, permits the deviatoric stress to intersect the failure envelope of sediments and soils.

Laboratory studies have helped to advance our understanding of the processes of liquefaction and to identify the major physical factors that affect liquefaction. However, it is difficult to duplicate natural conditions in the laboratory or to obtain undisturbed samples from the field. Thus, laboratory studies may have limited practical application. In the field, tests such as the 'standard' penetration test are employed to assess the liquefaction potential of specific sites. Despite their wide application, these tests are empirical. Thus, much progress can still be made toward a better physical understanding of the liquefaction process.

4.12.3 Observations and Their Explanations

Here, we review hydrologic phenomena that accompany earthquakes. We will see that the magnitudes of hydrologic changes caused by earthquakes are typically small enough to be of little human consequence. This is not always the case; however, depletion of groundwater induced by seismic activity has been invoked to explain the abandonment of regions of Crete, Greece, during the Late Minoan period (Gorokhovich, 2005), and mud eruptions, possibly triggered by earthquakes, can be devastating (Mazzini et al., 2007).

We categorize observations by type of observation (wells, streamflow, mud volcanoes, and geysers). It will also be helpful when discussing responses to distinguish hydrologic responses by the spatial relationship between the observation and the earthquake. We will use the terms near field, intermediate field, and far field for distances within one fault length, up to several fault lengths, and many fault lengths, respectively. In the near field, changes in the properties of the fault zone itself may be responsible for hydrologic responses. Examples include the formation of new springs along ruptured faults (e.g., Lawson, 1908) or changes in groundwater flow paths because of changes in the permeability of, or near, the fault zone (e.g., Gudmundsson, 2000). In both the near and intermediate fields, dynamic and static strains are large enough that they might cause a measurable hydrologic response. In the far field, however, only dynamic strains are sufficiently large to cause responses. In this chapter, we focus on hydrologic responses outside the fault zone.

Hydrologic changes following earthquakes modify pore pressures, which in turn can influence local seismicity. The topic of triggered seismicity is covered in the chapter by Hill and Prejean (**Chapter 4.11**), and we simply note here that the mechanisms responsible for the observed hydrologic phenomena discussed next may be connected to those responsible for distant, triggered seismicity.

4.12.3.1 Wells

The water level in wells measures the fluid pressure at depths where the well is open to the surrounding formations. Several types of coseismic and postseismic responses are observed: water-level oscillations, coseismic changes in water level, and delayed changes in water level. **Figure 3** shows a particularly dramatic example of a response in a well in which water erupted to a height of 60 m above the surface following the 2004 M9.2 Sumatra earthquake 3200 km away.

Figure 3 Well in China responding to the 2004 M9.2 Sumatra earthquake 3200 km away. The picture was taken by Hou Banghua, Earthquake Office of Meizhou County, Guangdong, 2 days after the Sumatra earthquake. The fountain was 50–60 m high when it was first sighted 1 day after the earthquake.

4.12.3.1.1 Water-level oscillations

Water wells can act like seismometers by amplifying ground motions, in particular long-period Rayleigh waves. Water-level fluctuations as large as 6 m (peak-to-peak amplitude) were recorded in Florida, thousands of kilometers away from the epicenter, during the 1964 Alaska earthquake (Cooper et al., 1965). Hydroseismograms have been recorded since the early days of seismometer use (Blanchard and Byerly, 1935).

Figure 4 (from Brodsky et al., 2003) shows water level in a well in Grants Pass, Oregon, following the 2002 M7.9 Denali earthquake 3100 km away. Also shown is the vertical component of ground velocity measured on a broadband seismometer located adjacent to the well. Large water-level fluctuations, such as those shown in **Figure 4**, are unusual and occur only for the right combination of geometric (water depth in the well, well radius, and aquifer thickness) and hydrologic properties (transmissivity). The frequency-dependent response of the water level in a well to dynamic strain in an aquifer can be determined theoretically by solving the coupled equations for pressure change in the aquifer, flow toward/away from the well, and flow within the well (e.g., Cooper et al., 1965; Liu et al., 1989). In general, high transmissivity favors large amplitudes.

Kono and Yanagidani (2006) found that in closed (as opposed to open) borehole wells, pore pressure variations are consistent with an undrained poroelastic response (see **Section 4.12.2.1**) at seismic frequencies. In addition, they found no pore pressure response to shear deformation.

4.12.3.1.2 Persistent and delayed postseismic changes in water level in the near and intermediate field

Persistent changes in water level in wells are probably the best-documented hydrologic responses to earthquakes. Significant advances in analysis of water-level changes following earthquakes have been made during the last decade by compiling observations, identifying patterns in responses, and using quantitative models to interpret the observations

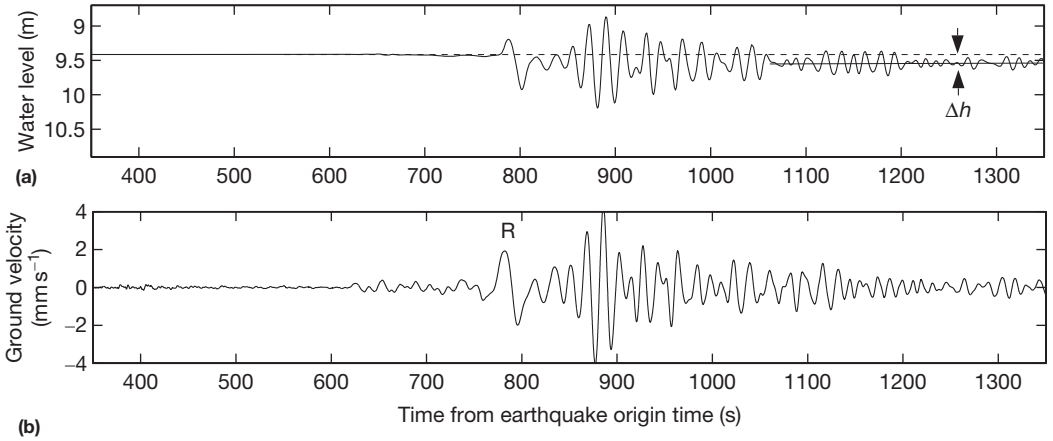

Figure 4 (a) Hydroseismograph recorded at 1 s intervals and (b) vertical component of ground velocity measured on a broadband seismometer at a well in Grants Pass, Oregon, following the 2002 M7.9 Denali earthquake located 3100 km away. Δh shows the 12 cm permanent change in water level that followed the passage of the seismic waves. *R* indicates the arrival of Rayleigh waves. Figure based on Figure 7 in Brodsky EE, Roeloffs E, Woodcock D, Gall I, and Manga M (2003) A mechanism for sustained ground water pressure changes induced by distant earthquakes. *Journal of Geophysical Research* 108: http://dx.doi.org/10.1029/2002JB002321.

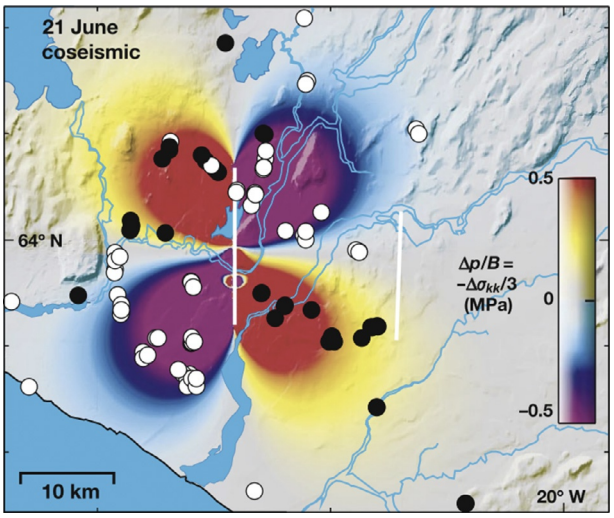

Figure 5 Predicted (color map) and observed (circles) coseismic water-level changes following a 2000 M6.5 strike-slip earthquake in Iceland. Black and white circles indicate water-level increases and decreases, respectively. The white line shows the mapped surface rupture. Figure from Jonsson S, Segall P, Pedersen R, and Bjornsson G (2003) Post-earthquake ground movements correlated to pore-pressure transients. *Nature* 424: 179–183.

(e.g., Brodsky et al., 2003; Chia et al., 2008; Cox et al., 2012; King et al., 1999; Kitagawa et al., 2006; Matsumoto and Roeloffs, 2003; Montgomery and Manga, 2003; Roeloffs, 1998; Roeloffs et al., 2003; Sato et al., 2004; Sil and Freymueller, 2006; Wang et al., 2003).

Sustained changes in water level in the near and possibly intermediate field can in some cases be explained by the coseismic static strain created by the earthquake. In this case, the water level will rise in zones of contraction and fall in regions of dilation.

Figure 5 (from Jonsson et al., 2003) shows a pattern of water-level change that mimics the pattern of coseismic volumetric strain after a strike-slip event in Iceland. An analogous correlation of volumetric strain and water-level changes was found after the 2003 M8.0 Tokachi-Oki thrust event in Japan (Akita and Matsumoto, 2004). Similar conclusions are reported by others (e.g., Quilty and Roeloffs, 1997; Wakita, 1975). This pattern of water-level change is not, however, universal. Following the 1999 M7.5 Chi-Chi earthquake in Taiwan, the water level rose in most near-field wells where the coseismic strain should have caused aquifer dilation (Koizumi et al., 2004; Wang et al., 2001). Following the 2004 M9 Sumatra earthquake, more than 5000 km away in Japan, Kitagawa et al. (2006) found that only about half the monitoring wells equipped with strain instruments recorded water-level changes consistent with the measured coseismic strain, implying that dynamic strains can also change water levels in the intermediate field.

Both the pattern and magnitude provide insight into the origin of water-level changes. The magnitude of expected water-level changes caused by coseismic strain can be determined from models of coseismic strain and models for well sensitivity that are calibrated on the basis of their response to barometric and tidal strains (e.g., Roeloffs, 1996). In some instances, recorded changes are similar to those predicted (e.g., Igarashi and Wakita, 1991), but changes can also be much larger than predicted, even in the near field (e.g., Igarashi and Wakita, 1995).

The time evolution of water-level changes provides additional constraints on the location and magnitude of pore pressure changes. **Figure 6** (from Roeloffs, 1998) shows water level for a period of 10 days following the 1992 M7.3 Landers earthquake 433 km from the well. The observed water-level changes, shown with data points, can be modeled by a coseismic, localized pore pressure change at some distance from the well (as shown by the solid curve). The origin, however, of the hypothesized pressure changes cannot be determined from measurements at the well (Roeloffs, 1998). Other processes that can cause delayed or gradual changes in water level are localized changes in porosity and/or permeability (e.g., Gavrilenko et al., 2000).

4.12.3.1.3 Near-field response of unconsolidated materials

At shallower depths and in unconsolidated materials, changes in water level in wells often exhibit larger amplitudes and different signs than predicted by the coseismic elastic strain. The 1999 Chi-Chi earthquake in Taiwan and, more recently, the 2010 Darfield earthquake in New Zealand provide excellent opportunities to examine models for postseismic water-level changes because the density of monitored wells was so high. We discuss these observations in much more detail than other types of well responses because the near-field hydrologic response at shallow depths and in unconsolidated materials is much less well studied. We focus, in our example, on the response to the Chi-Chi earthquake, because data for the New Zealand earthquakes are just appearing in the literature (Cox et al., 2012; Quigley et al., 2013) and there will undoubtedly be significant analyses appearing over the next few years.

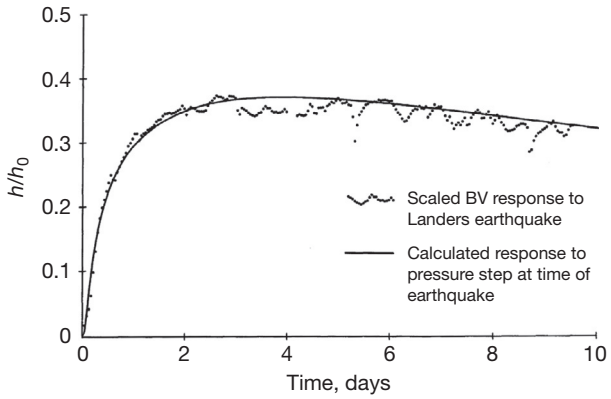

Figure 6 Water level as a function of time after the 1992 M7.2 Landers, CA, earthquake. The epicenter is 433 km away from the well. The smooth curve shows the predicted evolution of water level for a coseismic, localized pressure change at some distance from the well. h_0 is the magnitude of the head change where pore pressure changed. Figure from Roeloffs EA (1998) Persistent water level changes in a well near Parkfield, California, due to local and distant earthquakes. *Journal of Geophysical Research* 103: 869–889.

As a fortuitous coincidence, a network of 70 evenly distributed hydrologic stations (Figure 7), with a total of 188 wells, was installed in 1992 on a large alluvial fan (the Choshui River fan) near the Chi-Chi epicenter. The network was installed for the purpose of monitoring the groundwater resources over the Choshui River fan. At each station, one to five wells were drilled to depths ranging from 24 to 306 m to monitor groundwater level in individual aquifers. Each well was instrumented with a digital piezometer that automatically records the groundwater level hourly, with a precision of 1 mm (Hsu et al., 1999). The dense network of hydrologic stations and its close proximity to a large earthquake made the groundwater records during the Chi-Chi earthquake the most comprehensive and systematic so far obtained. In addition, a dense network of broadband strong-motion seismographic stations captured the ground motion in the area, and detailed studies of liquefaction occurrences were made. Finally, the isotopic composition of the groundwater was measured before and after the earthquake (Wang et al., 2005c).

The coseismic changes of groundwater level during this earthquake have been reported in several papers (Chia et al., 2001, 2008; Hsu et al., 1999; Lee et al., 2002; Wang et al., 2001). Near the ruptured fault, where consolidated sedimentary rocks occur near the surface, the groundwater level showed a coseismic, stepwise decrease (Figure 8(a) and 8(b)). Away from the ruptured fault, in the fan of unconsolidated sediments, confined aquifers showed a coseismic stepwise rise (Figure 8(c) and 8(d)). The magnitude of this rise increases with distance from the ruptured fault, reaching more than 5 m at distances of 20–30 km away from the fault before decreasing at greater distances (Figure 7(a); Wang et al., 2001). In the uppermost aquifer, the coseismic changes in the groundwater

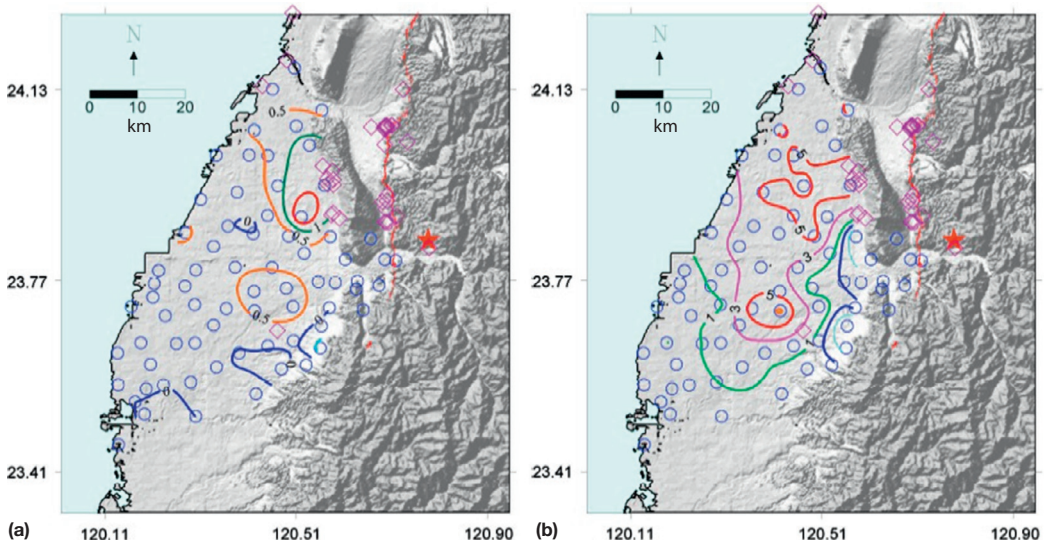

Figure 7 Spatial distribution of coseismic changes in groundwater level during the Chi-Chi earthquake. (a) Contours (m) showing coseismic groundwater-level changes in a confined aquifer (Aquifer II) in the Choshui River fan. (b) Contours (m) showing coseismic groundwater-level changes in the uppermost aquifer in the Choshui River fan. Groundwater monitoring stations are shown with open circles, liquefaction sites with open diamonds, epicenter of Chi-Chi earthquake with a star, and the ruptured fault with discontinuous red traces. Reproduced from Wang C-Y, Wang C-H, and Kuo C-Y (2004a) Temporal change in groundwater level following the 1999 (Mw = 7.5) Chi-Chi earthquake, Taiwan. *Geofluids* 4: 210–220.

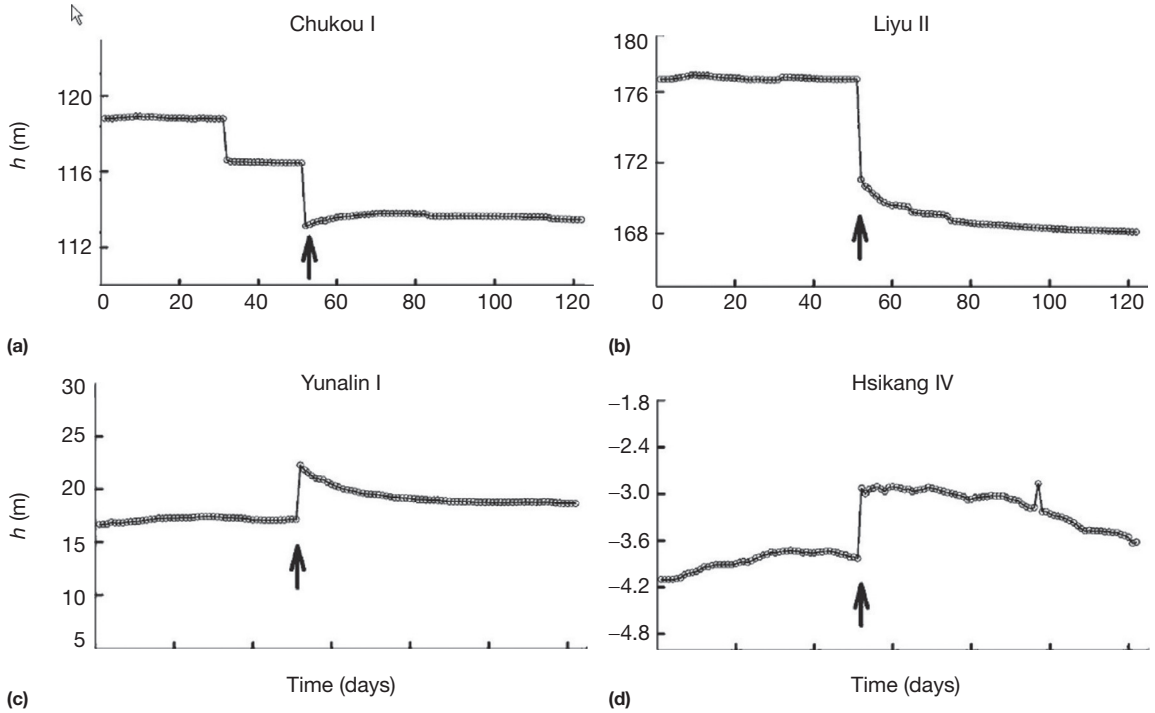

Figure 8 Four types of groundwater-level responses during the Chi-Chi earthquake. (a) Groundwater level dropped during the earthquake and gradually rose afterward. (b) Groundwater level dropped during the earthquake and continued to drop gradually afterward. (c) Groundwater level rose during the earthquake and gradually declined afterward. (d) Groundwater level rose during the earthquake and remained at the new level for some time before slowly declining. The different groundwater-level responses may be due to differences in the proximity to the ruptured fault and different hydrogeologic conditions as discussed in Wang et al. (2001). Figure created by Chung-Ho Wang.

level were much smaller in magnitude, with an irregular pattern (Figure 7(b)). Liquefaction sites on the Choshui River fan are clearly correlated with significant coseismic rise of the groundwater level in the uppermost aquifer; but no such correlation exists for the confined aquifers (Figure 7). This observation strongly indicates that liquefaction occurred in the uppermost aquifer but not in the confined aquifers. In the basins nearest the ruptured fault (east of the Choshui River fan), a comparison between liquefaction sites and the coseismic change in the groundwater level cannot be made, because no wells were installed and thus no groundwater-level data were available.

Lee et al. (2002) claimed that the spatial distribution of the groundwater-level change during the Chi-Chi earthquake may be accounted for by a poroelastic model. The widespread occurrence of liquefaction, however, provides clear evidence that at least part of the sediment deformation was not elastic. Furthermore, for confined aquifers that have a typical thickness of 1–10 m, the required changes in porosity would have to be from 10^{-3} to 10^{-2} to account for the range of coseismic groundwater-level changes (Wang et al., 2001), beyond the magnitude of strains calculated from an elastic model (Lee et al., 2002). Finally, the sign of the changes in water level is in general the opposite of those expected from a poroelastic model (Koizumi et al., 2004; Wang et al., 2001).

As noted earlier (Section 4.12.2.2), when loose sediments and soils are sheared at stresses between some upper and lower thresholds, grains tend to compact, leading to a decrease in porosity. If the deformation is undrained, as expected during seismic shaking, pore pressure would increase when the strain exceeds about 10^{-4}. This may explain the stepwise rise in the groundwater level in the fan (Figure 8(c) and 8(d)). On the other hand, when consolidated sediments or sedimentary rocks are cyclically sheared beyond some critical threshold, microfracture and fracture may occur, leading to increased porosity and permeability and decreased pore pressure. This may explain the coseismic decline in the groundwater level in sedimentary rocks close to the ruptured fault (Figure 8(a) and 8(b)).

It is possible to make an order-of-magnitude estimate of the change in porosity ϕ of the confined aquifer required to account for the coseismic water-level change. From the definition of specific storage $S = \rho^{-1}\partial(\rho\phi)/\partial h$ where h is the hydraulic head (Wang, 2000, p. 12), we have

$$\frac{\partial h}{\partial t} = \frac{1}{\rho S}\frac{\partial(\rho\phi)}{\partial t} \sim \frac{1}{S}\frac{\partial\phi}{\partial t} \qquad [10]$$

The term on the right-hand side of eqn [10] is the rate of change of sediment porosity at a given location resulting from ground shaking, which we assume is proportional to the intensity of ground shaking. Given that the intensity of ground shaking during the Chi-Chi earthquake decayed approximately exponentially with time (Ma et al., 1999), the rate of change in sediment porosity at a given location under earthquake shaking may be expressed as

$$\frac{d\phi}{dt} = Ae^{-\beta t} \qquad [11]$$

where β is on the order of $10^{-2} - 10^{-1}\,s^{-1}$ and A is a constant to be determined. Substituting eqn [11] into eqn [10] and

integrating with respect to time, we obtain the coseismic change in the hydraulic head:

$$\Delta h(t) = \frac{A}{S\beta}\left(e^{-\beta t} - 1\right) \qquad [12]$$

Pumping tests in the Choshui River fan yield $Sb \sim 10^{-3}$ (Lee and Wu, 1996) where b is the aquifer thickness. Given that ground shaking on the Choshui River fan during the Chi-Chi earthquake lasted between 20 and 100 s (Lee et al., 2002), for a 10 m groundwater-level change in a 1 m thick confined aquifer, $A = -10^{-4}$ to $-10^{-3}\,s^{-1}$, and for the same level of change in a 10 m aquifer, $A = -10^{-5}$ to $-10^{-4}\,s^{-1}$. We obtain a coseismic change in porosity between 10^{-3} and 10^{-2}.

The uppermost aquifer on the Choshui River fan is either unconfined or poorly confined, resulting in less regular changes in pore pressure and groundwater level. Thus, qualitatively, the processes of consolidation of sediments and dilation of sedimentary rocks, respectively, appear to provide a self-consistent interpretation of the spatial pattern of the coseismic groundwater-level changes on the Choshui River fan during the Chi-Chi earthquake (Wang et al., 2001).

The availability of both well records and strong-motion records at the time of the Chi-Chi earthquake allows quantitative examination of the relationship between ground motion, groundwater-level change, and the distribution of liquefaction sites. Interpolating the strong-motion parameters at the well sites, Wang et al. (2003) showed that there is only a weak correlation between the horizontal component of the peak ground acceleration (PGA) and the occurrence of water-level changes and liquefaction (**Figure 9(a)**). Wong and Wang (2007) confirmed this finding using a more extensive data set. This result is unexpected, because PGA is frequently used in engineering practice to predict the occurrence of liquefaction. Instead, Wong and Wang (2007) showed that there is a better correlation between the horizontal peak ground velocity (PGV) and the sites of liquefaction. Because PGV depends more on low-frequency components of ground motion than does PGA, this indicates that low-frequency ground motions are better correlated with elevated pore pressure and groundwater level than are high-frequency motions. This conclusion supports the finding that spectral accelerations and velocities at frequencies of about 1 Hz and lower were strongly correlated with the distribution of liquefaction sites (**Figure 9(b)**), whereas those above about 1 Hz were not (Wang et al., 2003; Wong and Wang, 2007). A similar conclusion was reached by comparing the hydrologic changes with various measures of earthquake intensity computed from seismograms passed through low-pass and high-pass filters (Wong and Wang, 2007). Although there is extensive evidence that low-frequency ground motions are better correlated with elevated pore pressure and groundwater level than high-frequency motions, it is unclear at this time whether the low-frequency ground motion was the cause for the coseismic groundwater-level change and liquefaction or whether the hydrologic changes, including liquefaction, caused the different spectral composition of the observed seismograms.

4.12.3.1.4 Intermediate-field and far-field response

In the far field (many fault lengths), the static stress due to the earthquake is nearly zero. Thus, sustained changes in water level at such distances (e.g., **Figure 4**) must be caused by the interactions between the aquifer and seismic waves. Such changes are not common, but occur at a small number of unusually sensitive sites usually located near active faults (King et al., 2006; Shi et al., 2014). The mechanism for these interactions is a matter of debate (Brodsky et al., 2003; Matsumoto and Roeloffs, 2003; Roeloffs, 1998).

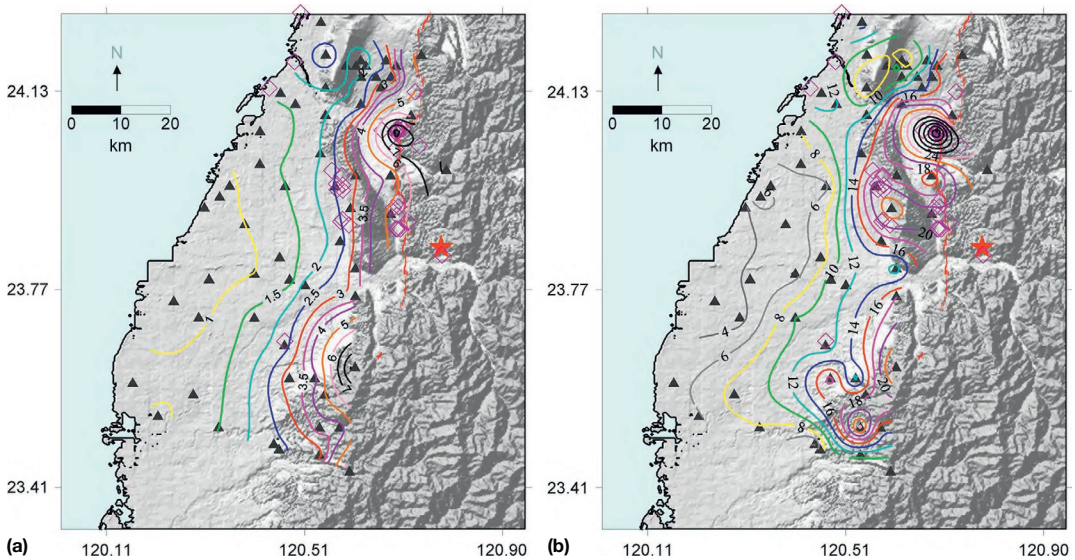

Figure 9 (a) Contours of the horizontal peak ground acceleration (PGA) during the Chi-Chi earthquake together with liquefaction sites in open diamonds. (b) Contours of the spectral acceleration at 1 Hz. The correlation of the occurrence of liquefaction with acceleration is better at 1 Hz than for the peak acceleration. See Wang et al. (2003) for a more detailed analysis. Modified from Wang C-Y, Dreger DS, Wang C-H, Mayeri D, and Berryman JG (2003) Field relations among coseismic ground motion, water-level change and liquefaction for the 1999 Chi-Chi (Mw = 7.5) earthquake, Taiwan. *Geophysical Research Letters* 17: http://dx.doi.org/10.1029/2003GL017601.

A permanent change in some aspect of pore structure is required, but the process by which small periodic strains change permeability or storage properties is unclear. Hydrogeochemical (e.g., Wang et al., 2004d) and temperature (e.g., Mogi et al., 1989; Wang et al., 2012; Wang et al., 2013) changes that accompany water-level changes confirm that pore-space connectivities change. One mechanism that has been proposed (to explain the particular postseismic change in water level shown in Figure 4) is that oscillatory flow back and forth in fractures caused by cyclic strain removes 'barriers' of fracture-blocking deposits, which then increases permeability and affects the final distribution of pore pressure (Brodsky et al., 2003). Elkhoury et al. (2006) confirmed that distant earthquakes can indeed change permeability. Earthquake-enhanced permeability does not seem to persist indefinitely. Manga et al. (2012) compiled observations of the timescale over which enhanced permeability returns to the preearthquake values. Timescales vary from as little as a few minutes (Geballe et al., 2011) to many years (e.g., Cappa et al., 2009; Kitagawa et al., 2007).

Other proposed, but also unverified, mechanisms include pore pressure increases caused by a mechanism 'akin to liquefaction' (Roeloffs, 1998), shaking-induced dilatancy (Bower and Heaton, 1978), or increasing pore pressure through seismically induced growth of bubbles (e.g., Linde et al., 1994). A feature of at least some far-field responses is that the magnitude of water-level changes scales with the amplitude of seismic waves (Sil and Freymueller, 2006).

One common feature of wells that exhibit far-field postseismic responses is that the sign of the water-level changes at a given well appears to be consistent among multiple earthquakes (Itaba and Koizumi, 2007; Matsumoto, 1992; Roeloffs, 1998; Sil and Freymueller, 2006). Any proposed mechanism should explain this feature, and the barrier explanation can only do so if the location of barriers is always located either up-gradient or down-gradient of the well. Wang and Chia (2008) suggested that this hypothesis makes a testable prediction that, if a sufficiently large number of observations are available, there should be a statistically random occurrence in both the sign and the magnitude of the water-level changes at a given epicentral distance. Using both a global set of water-level data and local data from Taiwan, Wang and Chia (2008) showed that there indeed appears to be such a statistically random occurrence. Far-field shaking-induced dilatancy (e.g., Bower and Heaton, 1978) or a process analogous to liquefaction (Roeloffs, 1998) would always cause the response to have the same sign, but neither can be universal mechanisms because the sign of water-level changes varies from well to well.

Observations from wells that have responded to multiple earthquakes indicate that wells may have an enhanced sensitivity over a specific range of frequencies (Roeloffs, 1998). Triggered earthquakes (Brodsky and Prejean, 2005), nonvolcanic tremor (Guilhem et al., 2010), liquefaction in the field (Holzer and Youd, 2007; Wong and Wang, 2007), and changes in eruption rate at mud volcanoes (Rudolph and Manga, 2012) all show increased sensitivity to long-period waves. Observations of, and models that account for, the frequency-dependent response may be useful for distinguishing between processes.

4.12.3.1.5 Summary

To generalize, on the basis of the reported changes in water level in the near and intermediate field, it appears that in general, deep wells in sound rock display a poroelastic response that mimics coseismic strain (in both sign and magnitude), whereas shallow wells and wells in poorly consolidated materials tend to show larger changes and increases in water level.

4.12.3.2 Streamflow

One of the most spectacular surface hydrologic responses to earthquakes is large changes in streamflow. Figure 10 shows two typical examples. The increased discharge is persistent, at least until rainfall obscures the changes caused by the earthquake. The peak discharge can occur from within a day to as much as several weeks after the earthquake. Increased streamflow occurs in the near and intermediate field (Manga, 2001). The total excess discharge (i.e., the total volume of water released in excess of that expected in the absence of the earthquake) can be large: 0.7 km^3 for the M7.5 Chi-Chi earthquake (Wang et al., 2004b) and 0.5 km^3 after the M7.5 Hebgen Lake earthquake (Muir-Wood and King, 1993). Because streamflow responds to precipitation in the drainage basin, earthquake-induced changes are best recorded and studied during the dry season or during dry periods when there is little or no precipitation.

Explanations for changes in streamflow can be divided into six categories: expulsion of deep crustal fluids resulting from coseismic elastic strain (e.g., Muir-Wood and King, 1993), changes in near-surface permeability (Briggs, 1991; Rojstaczer

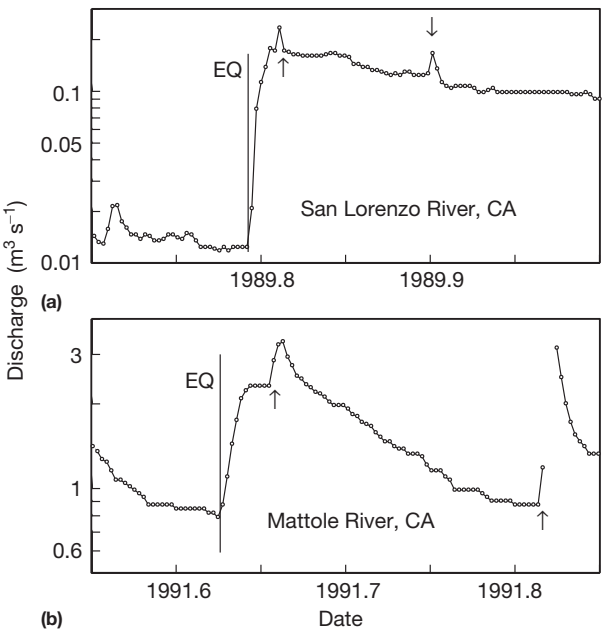

Figure 10 Hydrographs of (a) San Lorenzo River, CA, and (b) Mattole River, CA, showing postseismic response to the 1989 M7.3 Loma Prieta earthquake and 1991 M6 Honeydew earthquake, respectively. The vertical line labeled EQ indicates the time of the earthquake. Small arrows show the time of rainfall events. Figure made with US Geological Survey stream gauge data.

and Wolf, 1992; Rojstaczer et al., 1995; Sato et al., 2000; Tokunaga, 1999), consolidation or even liquefaction of near-surface deposits (Manga, 2001; Manga et al., 2003; Montgomery et al., 2003), release of water from the unsaturated zone (Manga and Rowland, 2009; Mohr et al., 2012), rupturing of subsurface reservoirs (Wang et al., 2004c), and the release of water trapped in fault zones. The differences between these different explanations are nontrivial because of their implications for the magnitude of crustal permeability, its evolution, and the nature of groundwater flow paths. We thus summarize the basis and some problems with each explanation and then consider the streamflow response to the 1999 Chi-Chi earthquake as an illustrative example:

1. Coseismic elastic strain

   Muir-Wood and King (1993) applied the coseismic elastic strain model, proposed by Wakita (1975) to explain coseismic groundwater-level changes, to explain the increased stream discharge after some large earthquakes, including the 1959 M7.5 Hebgen Lake earthquake and the 1983 M7.3 Borah Peak earthquake. Muir-Wood and King (1993) suggested that saturated microcracks in rocks were opened and closed in response to the stress change during an earthquake, causing pore volume to either increase or decrease, resulting in a decrease or increase in the groundwater discharge into streams.

   Following the 1989 Loma Prieta earthquake, however, chemical analysis of the stream water showed that the extra water that appeared in the streams following the earthquake had a shallow, rather than deep, origin (Rojstaczer and Wolf, 1992; Rojstaczer et al., 1995). Furthermore, Rojstaczer and colleagues showed that to account for the extra water in the increased streamflow by coseismic elastic strain, a very large volume of the crust must be involved in the expulsion of groundwater, which in turn would require an unreasonably high permeability for the crust. In addition, one important constraint on models is that streamflow generally increases, and the few streams with decreased discharge show very small changes.

   Manga et al. (2003) and Manga and Rowland (2009) reported that discharge increased at streams and springs in California after several earthquakes, irrespective of whether the coseismic strain in the basin was contraction or dilatation. For this reason, the dynamic strain caused by the earthquake, rather than the coseismic static strain, must be responsible for the observed changes in discharge, at least in the studied streams.

2. Enhanced permeability

   Briggs (1991) and Rojstaczer and Wolf (1992) and also Rojstaczer et al. (1995) proposed a model of enhanced permeability of the shallow crust resulting from seismically induced fractures and microfractures to explain the increased stream discharge in the nearby basins and the changes in the ionic concentration of stream water following the 1989 Loma Prieta earthquake in California. A shallow origin of the excess water is supported by a decrease in water temperature after discharge increased. Similar models were applied to the 1995 Kobe earthquake in Japan (Sato et al., 2000; Tokunaga, 1999) and the 2009 L'Aquila earthquake in Italy (Amoruso et al., 2011) to explain the observed hydrologic changes. Permeability enhancement was also invoked to explain increased electrical conductivity of water discharged after an earthquake (Charmoille et al., 2005). Elkhoury et al. (2006) found that earthquakes in Southern California caused phase shifts in the water-level response to tidal strain and interpreted these to be due to permeability increased by seismic waves. The increases in permeability are temporary; biogeochemical processes may act to reseal or block any newly created, fresh fractures.

   Manga (2001) found, however, that the rate of baseflow recession (i.e., the slow decrease in discharge during periods without precipitation) was unchanged by earthquakes that caused increases in streamflow. Assuming groundwater discharge Q to the stream is governed by Darcy's eqn [5], baseflow recession (a long time after recharge) is given by

$$\frac{dQ}{dt} \propto \exp[-aDt] \qquad [13]$$

   where a is a constant that characterizes the geometry of the drainage basin, D is the hydraulic diffusivity, and t is time. Although this is a great simplification of the complex subsurface flow paths of water to streams, such models in general provide an excellent empirical fit to discharge records. The slope of the hydrograph in **Figure 11(a)** is proportional to aD, and **Figure 11(b)** shows that the recession constant does not change following the earthquake. Given that the basin geometry and flow pathways are unlikely to have been reorganized by the earthquake, an unchanged baseflow recession implies that aquifer permeability did not change after the earthquake, even over the time period of increased discharge. This conclusion was substantiated by later studies in other areas (Montgomery et al., 2003) and during other earthquakes (Manga et al., 2003).

3. Coseismic consolidation and liquefaction

   Consolidation of loose materials is one way to increase pore pressures. Indeed, liquefaction occurred in many of the areas where streamflow increased (Montgomery and Manga, 2003). Consequently, Manga (2001) and also Manga et al. (2003) suggested that coseismic liquefaction of loose sediments on floodplains may provide the water for the increases in stream discharge following earthquakes.

   Figure 12 shows the relationship between earthquake magnitude and distance between the epicenter and the center of the gauged basin for streams that responded to earthquakes. Also shown for reference is the maximum distance over which liquefaction has been reported (from **Figure 2**). That the limit for both responses is similar does not imply that liquefaction causes streamflow to increase. Instead, the correlation simply means that dynamic strains sufficient to induce liquefaction under optimal conditions are also sufficient for streamflow to change.

   Wang et al. (2004b), however, used the extensive network of stream gauges in Taiwan to identify the source of excess discharge in streams. Excess discharge did not originate on the unconsolidated alluvial fan where there was, in fact, widespread liquefaction. Rather, the excess discharge originated in the mountains where there is little alluvial material and groundwater originated in bedrock.

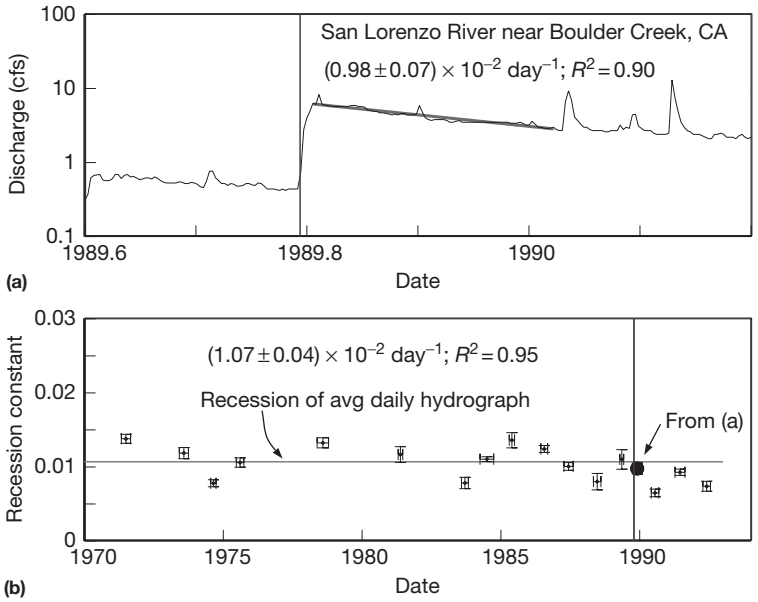

Figure 11 (a) Hydrograph of the San Lorenzo River, CA, showing postseismic response to the 1989 M7.3 Loma Prieta earthquake. The vertical line labeled EQ indicates the time of the earthquake. The postseismic period of baseflow recession is shown by the bold sloping line. (b) The baseflow recession constant for periods of baseflow before and after the earthquake showing that even though discharge increased by an order of magnitude, there was no significant change in baseflow recession. Figure made with US Geological Survey stream gauge data. Modified from Manga M (2001) Origin of postseismic streamflow changes inferred from baseflow recession and magnitude-distance relations. *Geophysical Research Letters* 28: 2133–2136.

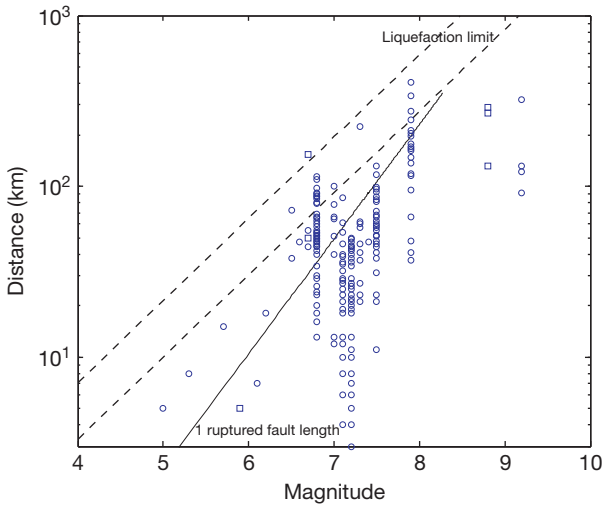

Figure 12 Relationship between earthquake magnitude and distance from the epicenter of streams that exhibited clear and persistent increases in discharge. Data shown with circles are from the compilation in Wang and Manga (2010a) with additional data shown with squares for the M8.8 Maule earthquake of 2010 (Mohr et al., 2012), the Tasso and Tanagro river responses to the M6.7 Irpinia, Italy, earthquake of 1930 (Esposito et al., 2009), and spring responses to the M5.9 Draney Peak, the United States, earthquake of 1994 (Schuster and Murphy, 1996). The dashed lines bound the maximum distance for liquefaction and the solid line is 1 ruptured fault length (see **Figure 2**).

In addition, after the 2001 M6.8 Nisqually, Washington, earthquake, Montgomery et al. (2003) did not find a significant field association between liquefaction occurrence and streamflow changes.

4. Water release from the unsaturated zone

   In some cases, excess discharge appears to originate from the unsaturated zone. Mohr et al. (2012) found that evapotranspiration and discharge both increased in small Chilean catchments after the M8.8 2010 Maule earthquake, suggesting that water drained from the unsaturated zone to the water table. Manga and Rowland (2009) noted that chloride concentrations and stable O and H isotopes in stream water after an earthquake were consistent with water that underwent significant evapotranspiration, a process that occurs in and near the unsaturated zone.

5. Fault valves and ruptured subsurface reservoirs

   In convergent tectonic regions, large volumes of pore water may be locked in subducted sediments (Townend, 1997). Sealing may be enacted partly by the presence of low-permeability mud and partly by the prevailing compressional stresses in such tectonic settings (Sibson and Rowland, 2003). Earthquakes may rupture the seals and allow pressurized pore water to erupt to the surface and recharge streams. This process may explain time variations in submarine fluid discharge at convergent margins (Carson and Screaton, 1998). Episodes of high discharge are correlated with seismic activity having features similar to tremor but are not correlated with large regional earthquakes (Brown et al., 2005).

   Following the M6.5 San Simeon, CA, earthquake on 22 December 2003, a different type of streamflow increase was revealed in the central Coast Ranges, occurring within 15 min of the earthquake and lasting about an hour. At the same time, several new hot springs appeared across a dry riverbed, a short distance upstream of the stream gauge that

registered the abrupt increase in streamflow. These observations suggest that the occurrence of streamflow increase and the appearance of hot springs were causally related and may be the result of earthquake-induced rupture of the seal of a hydrothermal reservoir. Recession analysis of the stream gauge data shows $D/L^2 \sim 1000\,s^{-1}$, where L is the depth of the reservoir, implying a small L or large D or both. Assuming a one-dimensional model for flow between the ruptured seal and the stream, Wang et al. (2004c) estimated that the extra discharge after this earthquake was $\sim 10^3\,m^3$. Abrupt changes in hot spring discharge are known to occur in the Long Valley, CA, hydrothermal area (Sorey and Clark, 1981), suggesting that this type of hydrologic response may be characteristic of hydrothermal areas.

Rupturing of permeability barriers may occur at depths of many kilometers. Husen and Kissling (2001) suggested that postseismic changes in the ratio of P-wave and S-wave velocities above the subducting Nazca Plate reflect fluid migration into the overlying plate following the rupture of permeability barriers. Disruption of low-permeability barriers by seismic waves generated $>10^4$ km away has been proposed (Doan and Cornet, 2007).

To illustrate some approaches that are used to test these explanations, we again consider the records from the 1999 M7.5 Chi-Chi earthquake in central Taiwan. In central Taiwan, 17 stream gauges are located on three stream systems (**Figure 13(a)**) that showed different responses to the 1999 Chi-Chi earthquake (Wang et al., 2004b). The local rainy season was over well before the earthquake. These records have made it possible to test the different hypotheses listed earlier. Among the three streams, two (Choshui Stream and the Wushi Stream) have extensive tributaries in the mountains (**Figure 13(a)**), but the third (Peikang Stream) originates on the sloping side of the Choshui fan, with no tributaries in the mountains. Streams in the mountains all showed large postseismic streamflow increases. On the alluvial fan, both the Choshui Stream and the Wushi Stream, which have tributaries in the mountains, showed large increases in streamflow. The amount of increase in streamflow in the proximal area of the Choshui alluvial fan was about the same as that in the distal area of the fan, indicating that most of the excess water originated in the mountains and that the contribution from the sediments in the fan was insignificant. By contrast, the Peikang Stream system, which does not have tributaries in the mountainous area, did not show any noticeable postseismic increase in streamflow. Thus, it may be concluded that the excess water in the streams after the Chi-Chi earthquake requires an earthquake-induced discharge from the mountains. Any coseismic consolidation and liquefaction of sediments on the floodplain (alluvial fan) were not substantial enough to cause noticeable postseismic increase in streamflow.

Figure 13(b) shows the discharge of a stream in the mountains before and after the Chi-Chi earthquake, together with the precipitation record from a nearby station. In addition to a coseismic increase in streamflow and a slow postseismic return to normal, the figure shows that the baseflow recession rates both before and after the earthquake are identical. This observation is of interest because it suggests that the Chi-Chi earthquake did not cause significant changes in the permeability of the aquifer that fed the stream, as Manga (2001) first noticed in

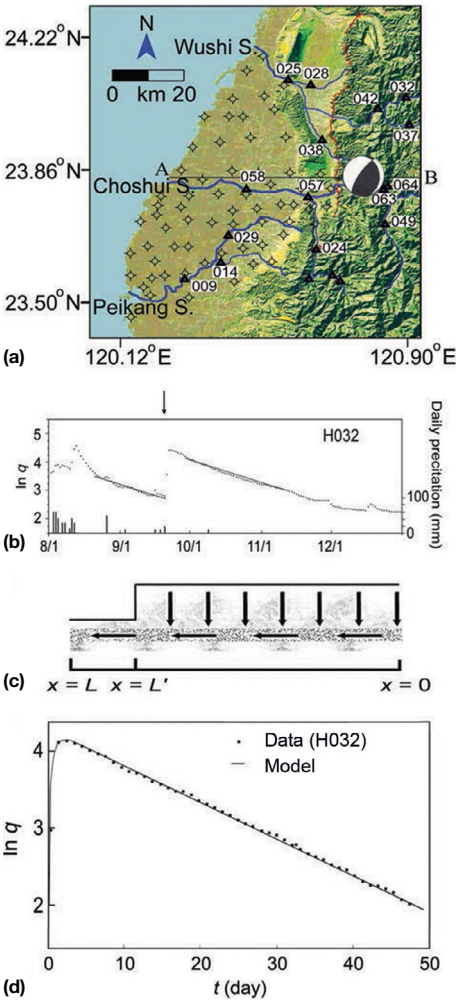

Figure 13 (a) Map showing the three river systems in central Taiwan and the locations of the stream gauges (triangles). Note that both the Wushi River and the Choshui River have extensive tributaries in the mountains, but the Peikang River does not. Hydrologic monitoring wells are marked by circles overlying crosses. (b) Logarithm of stream discharge as recorded by a gauge in central Taiwan as a function of time before and after the Chi-Chi earthquake, together with precipitation record at a nearby station. Note that the recession curve before and after the earthquake (indicated by arrow) has the same slope. (c) The conceptual model showing increased recharge of aquifer by groundwater from mountains due to enhanced vertical permeability during and after the earthquake. (d) Comparison of excess discharge as a function of time with model result (thin curve). Excess discharge at the time of earthquake ($t = 0$) is taken to be zero and therefore does not appear on the diagram.

his study of the coseismic responses of streams in the United States. However, the excess water in streams in central Taiwan after the Chi-Chi earthquake requires extra discharge from the mountains that can appear only through enhanced permeability during the earthquake. This apparent contradiction may be resolved by recognizing that the earthquake-induced change in permeability may be anisotropic. The foothills of the Taiwan mountains consist of alternating beds of sandstone and shale. Thus, before the earthquake, the vertical permeability would be controlled by the impervious shales and groundwater flow

would be mostly subhorizontal. During the earthquake, subvertical fractures breached the impervious shales and enhanced vertical permeability, allowing rapid downward draining of water to recharge underlying aquifers. The horizontal conductivity of the aquifers, which was high before the earthquake, was essentially unaffected. Field surveys after the Chi-Chi earthquake revealed numerous subvertical tensile cracks in the hanging wall of the thrust fault (Angelier et al., 2000; Lee et al., 2000, 2002). Many wells in the foothills above the thrust fault showed a significant drop in water level (Chia et al., 2001; Lin, 2000; Wang et al., 2001; Yan, 2001), and a sudden downpour occurred in a tunnel beneath the foothills right after the earthquake. Moreover, water temperatures decreased in wells located near the upper rim of the alluvial fan, as expected if vertical permeability and vertical groundwater flow increased (Wang et al., 2012). These observations are consistent with the model of enhanced vertical permeability during the Chi-Chi earthquake.

A one-dimensional leaky aquifer model (**Figure 13(c)**) may be used to quantify this conceptual model. Flow is governed by eqn [7], and the recharge to the aquifer resulting from enhanced vertical permeability is treated as a source. Even though this model is highly simplified, several studies (e.g., Brodsky et al., 2003; Manga, 2001; Manga et al., 2003; Roeloffs, 1998) have demonstrated that it is useful for characterizing the first-order response of hydrologic systems to earthquakes.

We treat the recharge of the leaky aquifer as coseismic with constant recharge for $0 < x \le L'$ (length of aquifer beneath the mountain with enhanced permeability) and no recharge for $L' > x > L$ (length of aquifer beneath the floodplain). If we further assume a boundary condition $h = 0$ at $x = L$ and a no-flow condition at $x = 0$, the excess discharge to the stream at time t is given by (e.g., Wang et al., 2004a)

$$Q_{ex} = \frac{2DVQ_0}{L^2(L'/L)} \sum_{n=1}^{\infty} (-1)^{n-1} \sin\left[\frac{(2r-1)\pi L'}{2L}\right] \exp\left[-\frac{(2r-1)^2\pi^2 D}{4L^2} t\right] \quad [14]$$

where L is the total length of the aquifer and V is the volume of the aquifer between $x = 0$ and $x = L'$ (**Figure 13(a)**); thus, VQ_0 is the total excess water recharging the aquifer. For large times, eqn [14] results in an exponential decrease in discharge, the so-called baseflow recession given by eqn [13]. **Figure 13(d)** compares the data for stream gauge 032 (adjusted to $Q_{ex} = 0$ just before the earthquake) with the modeled excess discharge Q_{ex} determined by eqn [14]. An excellent fit is obtained with $D/L^2 = 2.4 \times 10^{-7}\,s^{-1}$ (from recession analysis) and $L'/L = 0.8$. The latter value is consistent with the fact that gauge 032 is located in the mountains, where the floodplain is small in comparison with the total aquifer length. The amount of excess water VQ_0 may be determined from the value of DVQ_0/L^2 from model fitting. By summing the excess discharges in the Choshui Stream and in the Wushi Stream, we obtain a total amount of 0.7–0.8 km^3 for the excess water released from the mountains after the Chi-Chi earthquake.

For the example shown in **Figure 13**, the peak postseismic discharge occurs within a day of the earthquake. **Figure 14** shows an example in which the peak discharge is reached 9–10 days later, though discharge begins to increase

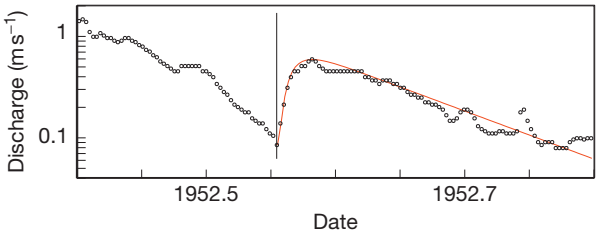

Figure 14 Response of Sespe Creek, CA, to the 1952 M7.5 Kern County earthquake. Daily discharge measurements collected and provided by the US Geological Survey are shown with circles. Curve is the solution to eqn [14] for the excess flow with $L'/L = 0.4$ added to the baseflow, eqn [13], to recover the entire hydrograph. Vertical line shows the time of the earthquake. There was no precipitation during the time interval shown in this graph.

coseismically. This example is for Sespe Creek, CA, responding to the 1952 M7.5 Kern County earthquake located 63 km away from the center of the drainage basin. Again, the model for excess discharge given by eqn [14], shown by the solid curve in **Figure 14**, fits the observed postseismic discharge very well (baseflow described by eqn [13] has been added back to the calculated excess discharge).

The different hypotheses listed in this section imply different crustal processes and different water–rock interactions during an earthquake cycle. In most instances, the hydrologic models are underconstrained. A reasonable approach is to test the different hypotheses against cases (such as Chi-Chi) in which abundant and accurate data are available. We note that a single explanation need not apply for all cases of increased streamflow so that identifying when and where different mechanisms dominate is important.

4.12.3.3 Mud Volcanoes

Mud volcanoes range from small, centimeter-size structures to large edifices up to few hundred meters high and several kilometers across. Mud volcanoes erupt predominantly water and fine sediment. They occur in regions where high sedimentation rates and fine-grained materials allow high pore pressures to develop (Kopf, 2002). Large mud volcanoes erupt from depths of several hundred meters to more than a couple kilometers.

Mud volcanoes also erupt in response to earthquakes (e.g., Panahi, 2005) and thus provide another probe of earthquake–hydrology interactions. Unfortunately, though, the number and quality of reports prevent a rigorous statistical analysis of the correlation (Bonini, 2009; Manga and Brodsky, 2006; Manga et al., 2009; Mellors et al., 2007).

A necessary condition to create mud volcanoes is the liquefaction or fluidization of erupted materials so that the erupted materials lose strength and can behave in a liquid-like manner (Pralle et al., 2003). Unconsolidated sediment can be liquefied and fluidized through mineral dehydration, gas expansion, tectonic stresses, inflow of externally derived fluids, and even ocean waves (Maltman and Bolton, 2003).

Figure 15 shows that the occurrence of triggered mud volcanism and changes in eruption rate falls within the liquefaction limit for shallow (upper few to tens of meters) liquefaction. The data shown in **Figure 15** are compiled and

tabulated in Wang and Manga (2010a) with additional data from Rudolph and Manga (2010, 2012), Manga and Bonini (2012), and Tsunogai et al. (2012).

Liquefaction is usually thought to be a shallow phenomenon confined to the upper few to tens of meters. This is because the fluid pressure needed to reach lithostatic pressure usually increases with depth. However, sedimentary basins with high sedimentation rates, fine sediments (with low permeability), and lateral compression often have high fluid pressures. Indeed, it is these settings in which mud volcanoes seem to occur (Milkov, 2000). Seismically triggered liquefaction may not necessarily be only a shallow phenomenon.

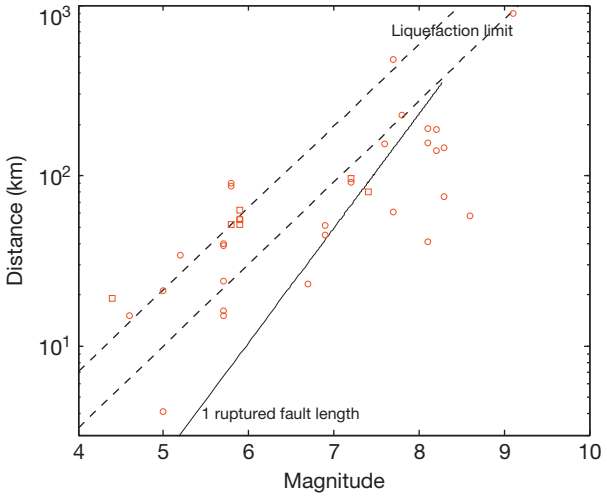

Figure 15 Relationship between earthquake magnitude, distance from the epicenter, and eruption of large mud volcanoes that originate from depths greater than hundreds of meters and erupted within a few days of the earthquake. Circles show data compiled and tabulated in Wang and Manga (2010a); squares show additional data from the Salton Sea, CA (Rudolph and Manga, 2010, 2012), the Northern Apennines, Italy (Manga and Bonini, 2012), and submarine mud volcanoes (Tsunogai et al., 2012). The dashed lines bound the maximum distance for liquefaction and the solid line is 1 ruptured fault length (see **Figure 2**).

Processes other than liquefaction have been invoked to explain the response of mud volcanoes and mud eruptions to earthquakes. Mazzini et al. (2009) appealed to reactivation of faults to enhance or create pathways to the surface that release overpressure. Rudolph and Manga (2012) showed that mud volcanoes are more sensitive to long-period waves of a given amplitude than short-period waves with the same amplitude. This supports mechanisms in which time-varying flows produced by seismic waves mobilize trapped bubbles (Beresnev et al., 2011) because bubble mobilization is more effective at low frequencies (Beresnev, 2006). Mobilizing or dislodging trapped bubbles has the effect of increasing permeability.

4.12.3.4 Geysers

Geysers change eruption frequency following distant earthquakes that generate coseismic static strains smaller than 10^{-7} or dynamic strains less than 10^{-6} (e.g., Hutchinson, 1985; Silver and Valette-Silver, 1992). Geysers, despite requiring very special thermal conditions and hydrogeologic properties to occur (Steinberg et al., 1982a), thus provide another opportunity to understand how earthquakes can influence hydrogeologic processes and properties.

Figure 16 shows the response of Daisy Geyser in Yellowstone National Park to the 2002 M7.9 Denali earthquake

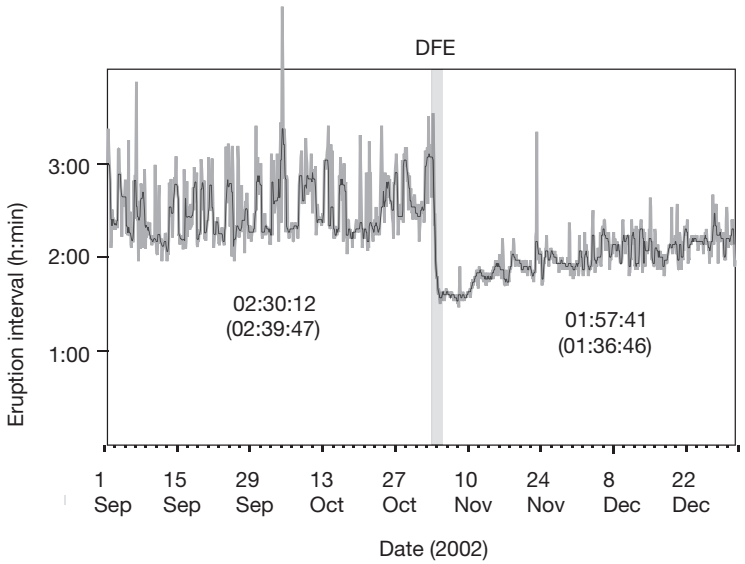

Figure 16 Eruption interval (time between two successive eruptions) in hour:minute format as a function of time at Daisy Geyser, Yellowstone National Park. Thin gray line shows raw data, that is, the actual measured eruption intervals. The black line is smoothed data obtained by averaging over several measurements. Median eruption intervals are also shown in hour/minute/second format. Median eruption intervals are computed over a several week period; intervals in parentheses are based on a few days before and after the earthquake. Time of the 2002 M 7.9 Denali earthquake is shown by the vertical line. Figure provided by Stephan Husen and made of data presented in Husen S, Taylor R, Smith RB, and Healser H (2004) Changes in geyser eruption behavior and remotely triggered seismicity in Yellowstone National Park produced by the 2002 M7.9 Denali fault earthquake, Alaska. *Geology* 32: 537–540.

located more than 3000 km away (Husen et al., 2004). The eruption interval decreases by about a factor of 2 and then slowly increases to the preearthquake frequency over a period of a few months. Among the many geysers at Yellowstone, the eruption frequency of some increased, whereas for others, it decreased.

Although geysers often respond to earthquakes, their response to barometric pressure changes (e.g., White, 1967), solid earth tides (e.g., Rinehart, 1972), and hypothetical preseismic strains (Silver and Valette-Silver, 1992) is weaker. The apparent correlation of eruption interval and nonseismic strains is, in fact, controversial. Rojstaczer et al. (2003) reanalyzed eruption records at Yellowstone and found that geysers were insensitive to earth tides and diurnal barometric pressure changes and thus concluded that geysers were not sensitive to strains less than about $10^{-8} - 10^{-7}$. One of these records was from Daisy Geyser (**Figure 16**). Given that Daisy Geyser responded to earthquakes that produced static strains as small as the amplitude of tidal strains, we can reasonably conclude that it is the larger amplitude dynamic strain, rather than static strain, that causes the observed responses (e.g., Husen et al., 2004).

The mechanism by which the eruption interval changes is not known. Steinberg et al. (1982b) noted that one mechanism for initiating a geyser eruption is superheating the water. Using a lab model of a geyser, Steinberg et al. (1982c) showed that vibrations can reduce the degree of superheating and can thus increase the eruption frequency. It is worth noting that while earthquakes can decrease the interval between eruptions, sometimes, the frequency of eruptions decreases. Ingebritsen and Rojstaczer (1993) proposed instead that much of the observed temporal variability in eruption frequency can be explained by changes in matrix permeability, which in turn governs the recharge of the conduit. Geyser frequency is also sensitive to the (often complex) conduit geometry (Hutchinson et al., 1997) and hence permeability of the geyser conduit. However, because the conduit is already much more permeable, small strains within the conduit itself are unlikely to have a significant effect on geyser eruptions (Ingebritsen et al., 2006). As a consequence, the observed temporal variability in eruption frequency is probably caused by changes in the permeability of the matrix surrounding the main geyser conduit – it is through this matrix that the conduit is recharged between eruptions.

The high sensitivity and long-lasting response of geysers to small seismic strains require reopening, unblocking, or creating fractures to induce large enough permeability changes to influence eruption frequency. Geysers thus provide evidence that dynamic strains are able to create permanent changes in permeability from small dynamic strains and at great distances from the earthquake.

In summary, the response of geysers to distant earthquakes is most easily explained by changes in permeability, and the sensitivity of geysers to earthquakes compared with earth tides and changes in barometric pressure indicates that dynamic strains cause the response.

4.12.4 Feedback Between Earthquakes and Hydrology

The presence of water in the subsurface, and changes in the amount of water on the surface or within the subsurface, can influence the occurrence of earthquakes, as summarized in **Figure 17**. There are three basic ways water can influence seismicity.

First, changes in loading of the surface can increase deviatoric stresses. The most clear examples follow the impoundment of water by reservoirs (e.g., Gupta, 1992; Simpson et al., 1988). Natural examples are more difficult to identify, probably in part because the magnitude of the surface load is much smaller; proposed examples include snow loading (Heki, 2003) and loading from ocean tides (Cochran et al., 2004) or other seasonal processes (Wolf et al., 1997).

Second, changes in fluid pressure p reduce the effective stress

$$\sigma_{ij}^{\text{eff}} = \sigma_{ij} - \alpha p \delta_{ij} \qquad [15]$$

where α is again the Biot–Willis coefficient. The classic example of seismicity induced by changes in pore pressure is earthquakes caused by fluid injection (e.g., Raleigh et al., 1976). Some cases of reservoir-induced seismicity, in particular those

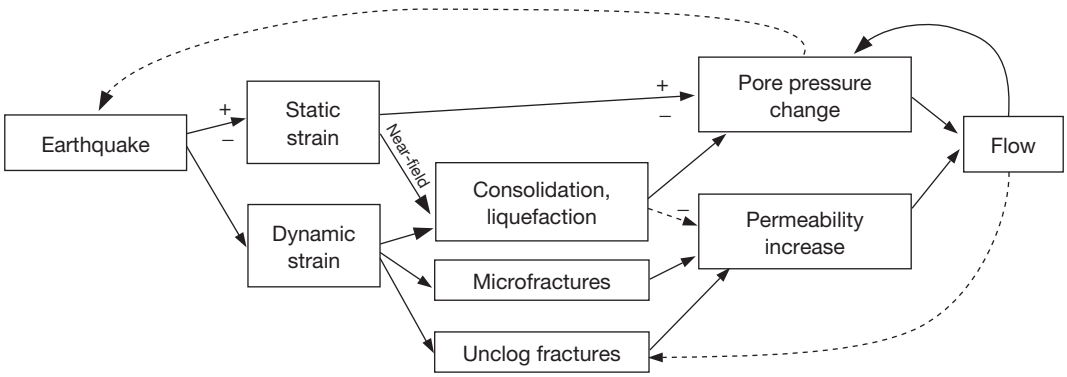

Figure 17 Schematic illustration of the relationship between earthquakes and hydrologic responses. + and – signs indicate the sign of the response. Figure based on an illustration originally created by David Mays. See Manga M, Beresnev I, Brodsky EE, Elkhoury JE, Elsworth DE, Ingebritsen S, Mays DC, and Wang C-Y (2012) Changes in permeability by transient stresses: Field observations, experiments and mechanisms. *Reviews of Geophysics* 50: RG2004, http://dx.doi.org/10.1029/2011RG000382.

in which the seismicity lags changes in water level, have been attributed to changes in pore pressure p (e.g., do Nascimento et al., 2005; Ge et al., 2009; Talwani and Acree, 1985). Changes in pore pressure also diffuse, governed by eqn [6], so the telltale signature of earthquakes triggered by changes in pore pressure would be a migration of the locus of seismicity at a rate consistent with the (usually unknown) hydraulic diffusivity. Spatial migration of reservoir-induced seismicity (Talwani and Acree, 1985), seismicity induced by fluid injection (Parotidis and Shapiro, 2004; Shapiro et al., 2006; Tadokoro et al., 2000), and some aftershock sequences (e.g., Bosl and Nur, 2002; Hainzl, 2004; Miller et al., 2004; Nur and Booker, 1972) have been attributed to pore pressure diffusion. Pore pressure changes caused by natural loading at the surface (e.g., groundwater recharge) have also been invoked to trigger seismicity (e.g., Christiansen et al., 2005, 2007; Costain et al., 1987; Hainzl et al., 2006; Saar and Manga, 2003).

Third, fluid extraction, rather than fluid injection, can change stresses through poroelastic deformation (Segall, 1989). Earthquakes appear to have been induced by fluid extraction in gas fields (Segall et al., 1994) and oil fields (Gomberg and Wolf, 1999; Zoback and Zinke, 2002). A decrease in pore pressure might be expected to stabilize faults by increasing the effective stress. Poroelastic deformation caused by changes in fluid pressure can, however, increase the magnitude of deviatoric stresses away from the region of fluid extraction.

One general conclusion from all these studies of hydrologically triggered seismicity, regardless of the mechanism, is that very small stress changes, typically 0.01–1 MPa, appear to trigger the earthquakes. Such small stress changes, however, are also similar to the stress changes thought to trigger earthquakes through nonhydrologic means (e.g., Harris, 1998; Stein, 1999).

If earthquakes cause changes in hydrogeologic properties and changes in fluid pressure promote seismicity, then hydrogeologic and seismological processes are coupled. Triggered seismicity (see review by Hill and Prejean; **Chapter 4.11**) is one possible example of this coupling. Interaction is promoted if the state of stress is close to failure so that the small changes in stress associated with either natural hydrologic processes or hydrologic responses to earthquakes can in turn influence seismicity. At least in tectonically active areas, many faults do appear to be critically stressed (Zoback et al., 1987), consistent with earthquakes being triggered by small stress changes.

Rojstaczer et al. (2008) suggested that one manifestation of this interaction is the value of the mean large-scale permeability of the crust – it should be of a size to accommodate internal forcing (fluid generation by metamorphic and magmatic processes) and external (groundwater recharge and discharge) forcing. Diagenesis, in general, tends to seal fractures and fill pores, thus decreasing permeability. If groundwater recharge does not change with time, water levels and pore pressures will increase, promoting seismicity, which in turn generates new fractures and increases permeability. A mean crustal permeability of 10^{-14}m^2 (Manning and Ingebritsen, 1999) is consistent with the present mean rate of groundwater recharge and hydraulic head gradients driving basin-wide groundwater flow. Rojstaczer et al. (2008) proposed that this balance is reached by a feedback between hydrologic processes and seismicity. A similar balance must occur in the lower crust, though the source of water is from metamorphic reactions rather than of meteorologic origin. The mean permeability obtained from such a balance, however, is a temporal and spatial average. Instead, evidence of short-lived and locally high permeabilities is preserved in the spatial distribution of mineral deposits in ancient fault systems (e.g., Micklethwaite and Cox, 2004) and transient, localized high temperatures in the lower crust (Camacho et al., 2005).

4.12.5 Hydrologic Precursors

As noted in **Section 4.12.2.1**, failure of brittle rocks under deviatoric stress is usually preceded by pervasive microcrack formation. In the subsurface, this process (i.e., microfracturing) would greatly increase the surface area of the affected rock in contact with groundwater and thus allow the release of gases and dissolved ions from the rock into the groundwater, changing its chemical composition. Coalescence of microcracks into larger fractures may connect hydraulically isolated aquifers, causing both changes in the hydraulic heads and mixing of groundwater with initially distinct hydrogeochemistry. These processes may further cause changes in the electrical conductivity of the rocks and thus of the crust. Scenarios of this kind have led to the not unreasonable expectation that hydrologic, hydrogeochemical, and related geophysical precursors may appear before the occurrence of large earthquakes.

During the 1960s and 1970s, several groups reported precursory changes in the crustal seismic velocity ratio (V_p/V_s) before some earthquakes in the then Soviet Union (Savarensky, 1968; Semenov, 1969), in New York (Aggarwal et al., 1973), and in California (Whitcomb et al., 1973). Scholtz et al. (1973) developed a dilatancy model as a common physical basis for precursory phenomena. Coupling the failure processes of brittle rocks with a groundwater flow model, Nur (1974) proposed a dilatancy model to explain the sequence of precursory changes in V_p/V_s. Later seismic experiments designed to detect changes in both V_p and V_s, however, failed to reveal any precursory changes before many major and moderate earthquakes (e.g., McEvilly and Johnson, 1974). In 1988, in response to Bakun and Lindh's (1985) prediction that a large earthquake would occur near Parkfield before 1993, Park installed a network of electrodes across the fault zone near Parkfield to detect any precursory changes in the electrical resistivity of the crust (Park, 1997) – one of the major predictions of the dilatancy model (Scholtz et al., 1973). The predicted Parkfield earthquake did not occur; but a M6.0 earthquake occurred on 28 September 2004, near Parkfield, providing an excellent opportunity to test the telluric method for detecting any precursory changes in crustal resistivity before a large earthquake. Careful data processing was applied to the time series of the dipole fields before the earthquake, but no precursory changes were found (Park, 2005). These failures, among others, have called into question the general validity of the dilatancy model, and about earthquake precursors in general.

A concerted search for hydrologic and hydrochemical precursors to earthquakes has also been pursued, and many candidates have been reported in the literature. For example, a few days prior to the 1946 M8.3 Nankaido earthquake in Japan,

water levels in some wells reportedly fell by more than 1 m and some wells went dry (Linde and Sacks, 2002; Sato, 1982). Three days before the 1985 M6.1 Kettleman Hills, CA, earthquake, Roeloffs and Quilty (1997) found a gradual, anomalous rise in water level of 3 cm. This observation was included in the IASPEI Preliminary List of Significant Precursors (Wyss and Booth, 1997). Following the 1995 M7.2 Kobe earthquake, several papers reported precursory changes in the concentrations of radon, chlorine, and sulfate ions in groundwater (e.g., Igarashi et al., 1995; Tsunogai and Wakita, 1995) and in groundwater level (King et al., 1995). Changes in radon concentration are the most commonly reported and discussed hydrogeochemical precursor (e.g., Trique et al., 1999; Wakita et al., 1988) because the release of radon is especially sensitive to crustal strains.

Definitive and consistent evidence for hydrologic and hydrochemical precursors, however, has remained elusive (Bakun et al., 2005; Wang and Manga, 2010a). There are many difficulties: Most reported changes were not corrected for the fluctuations in temperature, barometric pressure, earth tides, and other environmental factors, so that some changes taken to be earthquake-related may in fact be 'noise' (e.g., Hartman and Levy, 2005); changes were recorded at some sites but often were not recorded at other nearby sites (e.g., Biagi et al., 2001); instrument failures and personnel/program changes often do not allow persistent and consistent monitoring over long periods of time (King et al., 2000) – a necessary condition for obtaining reliable precursory data; it is technically challenging to perform continuous monitoring of chemical parameters (dissolved solids or gases), which might be more sensitive than easier-to-measure physical parameters such as water level, discharge, or temperature. Distinguishing a precursor from a response to a previous earthquake (e.g., the 1946 Nankaido earthquake mentioned in the previous paragraph was preceded by the 1944 M8.2 Tonankai event) creates additional ambiguity. Indeed, care is needed to distinguish a precursor from a hydrologic response. For example, Plastino et al. (2010) documented uranium groundwater anomalies at four sites prior to and after the 6th April Mw 6.3 L'Aquila, Italy, earthquake. They documented four excursions in uranium concentration at two sampling sites in the 10 months prior to the earthquake and then no excursions in the 2 months after the earthquake. Plastino et al. (2010) proposed that these excursions reflect strain in a preparatory phase. This interpretation, however, does not explain which anomalies will be followed by an earthquake, and the absence of postevent excursions (if real) could simply reflect postseismic changes. The latter is expected given that there were postseismic changes in stream and spring discharge.

Notwithstanding many difficulties, progress has been made in the past decade. For example, intensive and continued observations of various kinds of potential precursory hydrologic and hydrochemical changes have been made in Japan during the past half century (Wakita, 1996), and records are routinely corrected to remove the noise introduced by fluctuations in temperature, barometric pressure, earth tides, and other factors (Igarashi and Wakita, 1995); methods for filtering and time series analysis have been developed and applied to time series of raw hydrochemical and water-level data to remove changes unrelated to earthquake processes (Chen et al., 2010; Kingsley et al., 2001); and relationships among various types of hydrologic and hydrochemical precursory signals are being probed, as these would provide a better foundation for identifying and understanding any precursors (Hartman and Levy, 2005). It is now clear that long time series of observations are required: Claesson et al. (2007) found that an extended time series of geochemical measurements reduced the statistical significance of possible hydrogeochemical precursors they had previously postulated (Claesson et al., 2004). Although we may still be far from achieving a genuine understanding of the underlying mechanisms of the various earthquake-related anomalies, significant efforts are under way.

Static strains of 10^{-8} can reasonably be expected to produce changes in water level of about 1 cm for optimal hydrogeologic properties. Even greater sensitivity to strain (though perhaps only dynamic strains) is implied by some of the very distant hydrologic responses seen at geysers and some very distant changes in water in wells (e.g., Brodsky et al., 2003). The strong sensitivity of hydrologic processes and properties to small strains is the primary basis for hope that hydrologic and hydrogeochemical monitoring may detect any hypothetical preearthquake strains. Recognizing precursors, and distinguishing between responses from previous earthquakes and precursors to new earthquakes, is a different matter and may continue to be problematic (Hartman and Levy, 2005). Although it is unclear whether any future documented hydrologic precursors could actually be used for earthquake prediction, their occurrence or absence may at least provide new insight into the physics of earthquakes and the tectonic processes that lead to earthquakes.

4.12.6 Concluding Remarks

Hydrologic responses to earthquakes provide constraints on hydrogeologic processes in regions that might otherwise be inaccessible, for example, fault zones or the deep subsurface. Measured responses may also provide information at spatial and temporal scales that are difficult to study with more conventional hydrogeologic measurements such as well tests. However, these novel features of hydrologic responses also mean that it can be difficult, and perhaps even impossible in some cases, to obtain the information needed to distinguish between competing models for hydrologic responses.

Explaining the hydrologic responses to earthquakes should in principle be simple because they reflect the strain caused by earthquakes. The great variety of hydrologic responses, however, highlights the complexity of deformation and structure of geologic materials and the interaction among processes. Over the last decade, there has thus been a trend toward developing quantitative physically based models to explain hydrogeologic responses to earthquakes with an emphasis on explaining phenomena that cannot be explained by linear poroelastic models alone.

We conclude by noting that advances in physically based models may not be sufficient for understanding the interactions between earthquakes and water. Although expensive and time-consuming, continued monitoring of wells, springs, and streams, ideally at high sampling rates and with

complementary data sets (e.g., chemistry, temperature, and pressure), provides the data needed to test models and may also lead to the discovery of new hydrologic phenomena.

Acknowledgments

We thank Alex Wong, Fu-Qiong Huang, Maria Brumm, Emily Brodsky, Hiroo Kanamori, Steve Ingebrisen, and three reviewers for comments and suggestions, though none of these individuals should be held responsible for views and biases in this chapter. We also thank Fu-Qiong Huang for providing Figure 2 in this chapter. This is supported by the National Science Foundation.

References

Aggarwal YP, Sykes LR, Armbruster J, and Sbar ML (1973) Premonitory changes in seismic velocities and prediction of earthquakes. *Nature* 241: 101–104.

Akita F and Matsumoto N (2004) Hydrological responses induced by the Tokachi-oki earthquake in 2003 at hot spring well in Hokkaido, Japan. *Geophysical Research Letters* 31. http://dx.doi.org/10.1029/2004GL020433.

Ambraseys NN (1988) Engineering seismology. *Earthquake Engineering and Structural Dynamics* 17: 1–105.

Amoruso A, Crescentini L, Petitta M, Rusi R, and Tallini M (2011) Impact of the 6 April 2009 L'Aquila earthquake on groundwater flow in the Gran Sasso carbonate aquifer, Central Italy. *Hydrological Processes* 25: 1754–1764.

Andrew DJ (2003) A fault constitutive relation accounting for thermal pressurization of pore fluid. *Journal of Geophysical Research* 107. http://dx.doi.org/10.1029/2002JB001942.

Angelier J, Chu HT, Lee JC, et al. (2000) Geologic knowledge and seismic risk mitigation: Insight from the Chi-Chi earthquake – Taiwan. In: Lo C-H and Liao W-I (eds.) *Proceedings of International Workshop on Annual Commemoration of Chi-Chi Earthquake, Science Aspect*, pp. 13–24.

Arias A (1970) A measure of earthquake intensity. In: Hansen RJ (ed.) *Seismic Design for Nuclear Power Plant*, pp. 438–483. Cambridge, MA: Massachusetts Institute of Technology.

Bakun W and Lindh A (1985) The Parkfield earthquake prediction experiment. *Science* 229: 619–624.

Bakun WH, Aagaard B, Dost B, et al. (2005) Implications for prediction and hazard assessment from the 2004 Parkfield earthquake. *Nature* 437: 969–974.

Bardet JP (2003) Advances in analysis of soil liquefaction during earthquakes. In: Lee WHK, Kanamori H, Jennings PC, and Kisslinger C (eds.) *International Handbook of Earthquake and Engineering Seismology, Part B*, pp. 1175–1201. San Diego, CA: Academic Press.

Beresnev IA (2006) Theory of vibratory mobilization of nonwetting fluids entrapped in pore constrictions. *Geophysics* 71: N47–N56.

Beresnev IA, Gaul W, and Vigil RD (2011) Direct pore-level observation of permeability increase in two-phase flow by shaking. *Geophysical Research Letters* 38: L20302.

Berryman JG and Wang HF (2000) Elastic wave propagation and attenuation in a double-porosity dual-permeability medium. *International Journal of Rock Mechanics and Mining Sciences* 37: 67–78.

Biagi PF, Ermini A, Kingsley SP, Khatkevich YM, and Gordeev EI (2001) Difficulties with interpreting changes in groundwater gas content as earthquake precursors in Kamchatka, Russia. *Journal of Seismology* 5: 487–497.

Biot MA (1941) General theory of three-dimensional consolidation. *Journal of Applied Physics* 12: 155–164.

Biot MA (1956a) Theory of propagation of elastic waves in fluid-saturated porous solid. I. Low-frequency range. *Journal of the Acoustical Society of America* 28: 168–178.

Biot MA (1956b) Theory of propagation of elastic waves in fluid-saturated porous solid. I. Higher frequency range. *Journal of the Acoustical Society of America* 28: 179–191.

Biot MA (1962) Mechanics of deformation and acoustic propagation in porous media. *Journal of Applied Physics* 33: 1482–1498.

Bird P (1978) Stress and temperature in subduction shear zones: Tonga and Mariana. *Geophysical Journal of the Royal Astronomical Society* 55: 411–434.

Blanchard FB and Byerly P (1935) A study of a well gauge as a seismograph. *Bulletin of the Seismological Society of America* 25: 313–321.

Bonini M (2009) Mud volcano eruptions and earthquakes in the Northern Apennines and Sicily, Italy. *Tectonophysics* 474: 723–735.

Bosl WJ and Nur A (2002) Aftershocks and pore fluid diffusion following the 1992 Landers earthquake. *Journal of Geophysical Research* 107: 2366.

Bower DR and Heaton KC (1978) Response of an aquifer near Ottawa to tidal forcing and the Alaskan earthquake of 1964. *Canadian Journal of Earth Sciences* 15: 331–340.

Brace WF, Paulding J, and Scholz C (1966) Dilatancy in the fracture of crystalline rocks. *Journal of Geophysical Research* 71: 3939–3953.

Briggs RO (1991) Effects of Loma Prieta earthquake on surface water in Waddell Valley. *Water Resources Bulletin* 27: 991–999.

Brodsky EE and Kanamori H (2001) Elastohydrodynamic lubrication of faults. *Journal of Geophysical Research* 106: 16357–16374.

Brodsky EE and Prejean SG (2005) New constraints on mechanisms of remotely triggered seismicity at Long Valley Caldera. *Journal of Geophysical Research* 110. http://dx.doi.org/10.1029/2004JB003211.

Brodsky EE, Roeloffs E, Woodcock D, Gall I, and Manga M (2003) A mechanism for sustained ground water pressure changes induced by distant earthquakes. *Journal of Geophysical Research* 108. http://dx.doi.org/10.1029/2002JB002321.

Brodsky EE, Mori J, and Fulton PM (2010) Drilling into faults quickly after earthquakes. *Eos, Transactions American Geophysical Union* 91: 23744. http://dx.doi.org/10.1029/2010EO270001.

Brown KM, Tryon MD, DeShon HR, Schwartz S, and Dorman LM (2005) Correlated transient fluid pulsing and seismic tremor in the Costa Rica subduction zone. *Earth and Planetary Science Letters* 238: 189–203.

Camacho A, Lee JKW, Hensen BJ, and Braun J (2005) Short-lived orogenic cycles and the eclogitization of cold crust by spasmodic hot fluids. *Nature* 435: 1191–1196.

Cappa F, Rutqvist J, and Yamamoto K (2009) Modeling crustal deformation and rupture processes related to upwelling of deep CO_2-rich fluids during the 1965–1967 Matsushiro earthquake swarm in Japan. *Journal of Geophysical Research* 114: B10304. http://dx.doi.org/10.1029/2009JB006398.

Carson B and Screaton EJ (1998) Fluid flow in accretionary prisms: Evidence for focused, time-variable discharge. *Reviews of Geophysics* 36: 329–352.

Chen CH, et al. (2010) Identification of earthquake signals from groundwater level records using the HHT method. *Geophysical Journal International* 180: 1231–1241.

Chia YP, et al. (2008) Implications of coseismic groundwater level changes observed at multiple-well monitoring stations. *Geophysical Journal International* 172: 293–301.

Charmoille A, Fabbri O, Mudry J, Guglielmi Y, and Bertrand C (2005) Post-seismic permeability change in a shallow fractured aquifer following a M-L 5.1 earthquake (Fourbanne karst aquifer, Jura outermost thrust unit, eastern France). *Geophysical Research Letters* 32: L18406.

Chester FM, Evens JP, and Biegel RL (1993) Internal structure and weakening mechanisms of the San Andreas fault. *Journal of Geophysical Research* 98: 771–786.

Chester FM, Chester JS, Kirschner DL, Schulz SE, and Evans JP (2004) Structure of large-displacement strike-slip fault zones in the brittle continental crust. In: Karner GD, Taylor B, Driscoll NW, and Kohlstedt DL (eds.) *Rheology and Deformation in the Lithosphere at Continental Margins*, pp. 223–260. New York: Columbia University Press.

Chia YP, Wang YS, Wu HP, Chiu JJ, and Liu CW (2001) Changes of groundwater level due to the 1999 Chi-Chi earthquake in the Choshui River fan in Taiwan. *Bulletin of the Seismological Society of America* 91: 1062–1068.

Christiansen LB, Hurwitz S, and Ingebritsen SE (2007) Annual modulation of seismicity along the San Andreas Fault near Parkfield. *Geophysical Research Letters* 34: L04306. http://dx.doi.org/10.1029/2006GL028634.

Christiansen LB, Hurwitz S, Saar MO, Ingebritsen SE, and Hsieh PA (2005) Seasonal seismicity at western United States volcanic centers. *Earth and Planetary Science Letters* 240: 307–321.

Chu C-L, Wang C-Y, and Lin W (1981) Permeability and frictional properties of San Andreas fault gouges. *Geophysical Research Letters* 8: 56568. http://dx.doi.org/10.1029/GL008i006p00565.

Claesson L, Skelton A, Graham C, et al. (2004) Hydrogeochemical changes before and after a major earthquake. *Geology* 32L: 641–644.

Claesson L, Skelton A, Graham C, and Morth C-M (2007) The timescale and mechanisms of fault sealing and water–rock interaction after an earthquake. *Geofluids* 7: 427–440.

Cochran ES, Vidale JE, and Tanaka S (2004) Earth tides can trigger shallow thrust fault earthquakes. *Science* 306: 1164–1166.

Cooper HH, Bredehoeft JD, Papadopulos IS, and Bennett RR (1965) The response of well-aquifer systems to seismic waves. *Journal of Geophysical Research* 70: 3915–3926.

Costain JK, Bollinger GA, and Speer JA (1987) Hydroseismicity: A hypothesis for the role of water in the generation of intraplate seismicity. *Seismological Research Letters* 58: 41–64.

Cox SC, Rutter HJ, Sims A, et al. (2012) Hydrological effects of the Darfield (Canterbury) Mw 7.1 earthquake, 4 September 2010, New Zealand. *New Zealand Journal of Geology and Geophysics* 55: 231–247.
do Nascimento AF, Lunn RJ, and Cowie PA (2005) Numerical modelling of pore-pressure diffusion in a reservoir-induced seismicity site in northeast Brazil. *Geophysical Journal International* 160: 249–262.
Doan ML and Cornet FH (2007) Small pressure drop triggered near a fault by small teleseismic waves. *Earth and Planetary Science Letters* 258: 207–218.
Dobry R (1989) Some basic aspects of soil liquefaction during earthquakes. *Annals of the New York Academy of Sciences* 558: 172–182.
Dvorkin J, Nolen-Hoeksema R, and Nur A (1994) The squirt-flow mechanism: Macroscopic description. *Geophysics* 59: 428–438.
Esposito E, Pece R, Porfido S, and Tranfaglia G (2009) Ground effects and hydrological changes in Southern Apennines (Italy) in response to the 23 July 1930 earthquake (Ms = 6.7). *Natural Hazards and Earth System Sciences* 9: 539–550.
Elkhoury JE, Brodsky EE, and Agnew DC (2006) Seismic waves increase permeability. *Nature* 441: 1135–1138.
Forster CB, Evens JP, Tanaka H, Jeffreys R, and Noraha T (2003) Hydrologic properties and structure of the Mozumi Fault, central Japan. *Journal of Geophysical Research* 30. http://dx.doi.org/10.1029/2002GL014904.
Galli P (2000) New empirical relationships between magnitude and distance for liquefaction. *Tectonophysics* 324: 169–187.
Gavrilenko P, MeliKadze G, Chelidze T, Gibert D, and Kumsiashvili G (2000) Permanent water level drop associated with the Spitak earthquake: Observations at Lisi borehole (Republic of Georgia) and modelling. *Geophysical Journal International* 143: 83–98.
Ge S, Liu M, Lu N, Godt LW, and Luo G (2009) Did the Zipingpu Reservoir trigger the 2008 Wenchuan earthquake? *Geophysical Research Letters* 36: L20315. http://dx.doi.org/10.1029/2009GL040349.
Geballe ZM, Wang CY, and Manga M (2011) A permeability-change model for water level changes triggered by teleseismic waves. *Geofluids* 11: 302–308.
Gomberg J and Wolf L (1999) A possible cause for an improbable earthquake: The 1997 Mw 4.9 southern Alabama earthquake and hydrocarbon recovery. *Geology* 27: 367–370.
Gorman P (2011) Scientists poised to drill into fault: Science/Stuff.co.nz (http://www.stuff.co.nz/science/4511807/Scientists-poised-to-drillinto-fault).
Gorokhovich Y (2005) Abandonment of Minoan palaces on Crete in relation to the earthquake induced changes in groundwater supply. *Journal of Archaeological Science* 32: 217–222.
Gudmundsson A (2000) Active fault zones and groundwater flow. *Geophysical Research Letters* 27: 2993–2996.
Guilhem A, Peng Z, and Nadeau RM (2010) High-frequency identification of non-volcanic tremor triggered by regional earthquakes. *Geophysical Research Letters* 37: L16309. http://dx.doi.org/10.1029/2010GL044660.
Gupta HK (1992) *Reservoir-Induced Earthquakes*, 264 pp. New York: Elsevier.
Hainzl S (2004) Seismicity patterns of earthquake swarms due to fluid intrusion and stress triggering. *Geophysical Journal International* 159: 1090–1096.
Hainzl S, Kraft T, Wassermann J, Igel I, and Schmedes E (2006) Evidence for rainfall-triggered earthquake activity. *Geophysical Research Letters* 33: L19303. http://dx.doi.org/10.1029/2006GL027642.
Hamiel Y, Lyakhovsky V, and Agnon A (2005) Rock dilation, nonlinear deformation, and pore pressure change under shear. *Earth and Planetary Science Letters* 237: 577–589.
Hancox GT, Cox SC, Turnbull IM, and Crozier MJ (2003) Landslides and other ground damage caused by the Mw 7.2 Miordland earthquake of 22 August 2003. Institute of Geological and Nuclear Sciences, Science Report 2003/30, Lower Hutt.
Harris RA (1998) Introduction to the special section: Stress triggers, stress shadows, and the implication for seismic hazard. *Journal of Geophysical Research* 103: 24247–24258.
Hartman J and Levy JK (2005) Hydrogeological and gasgeochemical earthquake precursors – A review for application. *Natural Hazards* 34: 279–304.
Heki K (2003) Snow load and seasonal variation of earthquake occurrence in Japan. *Earth and Planetary Science Letters* 207: 159–164.
Holzer TL and Youd TL (2007) Liquefaction, ground oscillation, and soil deformation at the Wildlife Array, California. *Bulletin of the Seismological Society of America* 97: 961–976.
Hsu SK, Chin CV, Cheng LH, and Lin WS (1999) The change of groundwater level of earthquake 921 in central Taiwan. In: *Proceedings of Conference on Sustainable Development and Geosciences Prospect: National Taiwan University, Department of Geology,* pp. 7–35 (in Chinese).
Husen S and Kissling E (2001) Postseismic fluid flow after the large subduction earthquake of Antofagasta, Chile. *Geology* 29: 847–850.
Husen S, Taylor R, Smith RB, and Healser H (2004) Changes in geyser eruption behavior and remotely triggered seismicity in Yellowstone National Park produced by the 2002 M 7.9 Denali fault earthquake, Alaska. *Geology* 32: 537–540.
Hutchinson RA (1985) Hydrothermal changes in the upper geyser basin, Yellowstone National Park, after the 1983 Borah Peak, Idaho, earthquake. USGS Open File Report 85-290, 612–624.
Hutchinson RA, Westphal JA, and Kieffer SW (1997) In situ observations of Old Faithful Geyser. *Geology* 25: 875–878.
Igarashi G and Wakita H (1991) Tidal responses and earthquake-related changes in the water level of deep wells. *Journal of Geophysical Research* 96: 4269–4278.
Igarashi G and Wakita H (1995) Geochemical and hydrological observations for earthquake prediction in Japan. *Journal of Physics of the Earth* 43: 585–598.
Igarashi G, Saeki S, Takahata N, et al. (1995) Ground-water radon anomaly before the Kobe earthquake in Japan. *Science* 269: 60–61.
Ingebritsen SE and Rojstaczer SA (1993) Controls on geyser periodicity. *Science* 262: 889–892.
Ingebritsen SE, Sanford WE, and Neuzil CE (2006) *Groundwater in Geologic Processes*, 2nd edn., 562 pp. New York: Cambridge University Press.
Ishihara K (1996) *Soil Behavior in Earthquake Geotechnics*, 350 pp. Oxford: Clarendon Press.
Itaba S and Koizumi N (2007) Earthquake-related changes in groundwater levels at the Dogo hot spring, Japan. *Pure and Applied Geophysics* 164: 2397–2410.
Jennings PC (2003) An introduction to the earthquake response of structures. In: Lee WHK, Kanamori H, Jennings PC, and Kisslinger C (eds.) *International Handbook of Earthquake and Engineering Seismology, Part B*, pp. 1097–1126. London: Academic Press.
Jonsson S, Segall P, Pedersen R, and Bjornsson G (2003) Post-earthquake ground movements correlated to pore-pressure transients. *Nature* 424: 179–183.
King C-Y, Koizumi N, and Kitagawa Y (1995) Hydrogeochemical anomalies and the 1995 Kobe earthquake. *Science* 269: 38–39.
King C-Y, Azuma S, Igarashi G, Ohno M, Saito H, and Wakita H (1999) Earthquake-related water-level changes at 16 closely clustered wells in Tono, central Japan. *Journal of Geophysical Research* 104: 13073–13082.
King C-Y, Azuma S, Ohno M, et al. (2000) In search of earthquake precursors in the water-level data of 16 closely clustered wells at Tono, Japan. *Geophysical Journal International* 143: 469–477.
King CY, Zhang W, and Zhang ZC (2006) Earthquake-induced groundwater and gas changes. *Pure and Applied Geophysics* 163: 633–645.
Kingsley SP, Biagi PF, Piccolo R, et al. (2001) Hydrogeochemical precursors of strong earthquakes: A realistic possibility in Kamchatka. *Physics and Chemistry of the Earth, Part C* 26: 769–774.
Kitagawa Y, Fujimori K, and Koizumi N (2007) Temporal change in permeability of the Nojima Fault zone by repeated water injection experiments. *Tectonophysics* 443: 18392.
Kitagawa Y, Koizumi N, Takahashi M, Matsumoto N, and Sato T (2006) Changes in groundwater levels or pressures associated with the 2004 earthquake off the west coast of northern Sumatra (M 9.0). *Earth, Planets and Space* 58: 173–179.
Koizumi N, Lai W-C, Kitagawa Y, and Matsumoto N (2004) Comment on "Coseismic hydrological changes associated with dislocation of the September 21, 1999 Chichi earthquake, Taiwan" In: Lee M, et al. (eds.) *Geophysical Research Letters* 31. http://dx.doi.org/10.1029/2004GL019897.
Kono Y and Yanagidani T (2006) Broadband hydroseismograms observed by closed borehole wells in the Makioka mine, central Japan: Response of pore pressure to seismic waves from 0.05 to 2 Hz. *Journal of Geophysical Research* 111: B03410.
Kopf AJ (2002) Significance of mud volcanism. *Reviews of Geophysics* 40. http://dx.doi.org/10:1029/2000RG000093.
Kuribayashi E and Tatsuoka F (1975) Brief review of liquefaction during earthquakes in Japan. *Soils and Foundations* 15: 81–92.
Lachenbruch A (1980) Frictional heating, fluid pressure, and the resistance to fault motion. *Journal of Geophysical Research* 85: 6097–6112.
Lachenbruch AH and Sass JH (1977) Heat flow in the United States and the thermal regime of the crust. In: Heacock JH (ed.) *The Earth's Crust. Geophysical Monograph Series*, vol. 20, pp. 625–675. Washington, DC: American Geophysical Union.
Lawson AC (1908) The California Earthquake of April 18, 1906. *Report of the State Earthquake Investigation Commission*, vol. 1. Washington, DC.: Carnegie Institution of Washington.
Lay T and Wallace TC (1995) *Modern Global Seismology*. Academic Press.
Lee CS and Wu CL (1996) Pumping tests of the Choshuichi alluvial fan. In: *Conference on Groundwater and Hydrology of the Choshui River Alluvial Fan, Taiwan, Water Resources Bureau,* pp. 165–179 (in Chinese).
Lee CT, Kelson KI, and Kang KH (2000) Hanging wall deformation and its effect on buildings and structures as learned from the Chelungpu faulting in the 1999

Chi-Chi Taiwan earthquake. In: Lo C-H and Liao W-I (eds.) *Proceedings of International Workshop Annual Commemoration of Chi-Chi Earthquake, Science Aspect*, pp. 93–104.

Lee J-C, Chu H-T, Angelier J, et al. (2002a) Geometry and structure of northern rupture surface ruptures of the 1999 Mw = 7.6 Chi-Chi Taiwan earthquake: Influence from inherited fold belt structures. *Journal of Structural Geology* 24: 173–192.

Lee M, Liu T-K, Ma K-F, and Chang Y-M (2002) Coseismic hydrological changes associated with dislocation of the September 21, 1999 Chi-Chi earthquake, Taiwan. *Geophysical Research Letters* 29. http://dx.doi.org/10.1029/2002GL015116.

Li Y-G and Malin PE (2008) San Andreas Fault damage at SAFOD viewed with fault-guided waves. *Geophysical Research Letters* 35: L08304. http://dx.doi.org/10.1029/2007GL032924.

Li H and Zhu L (2007) High-resolution structures of the Landers fault zone inferred from aftershock waveform data. *Geophysical Journal International* 171: 1295–1307.

Li Y-G, Vidale JE, Aki K, and Xu F (2000) Depth-dependent structure of the Landers Fault zone from trapped waves generated by aftershocks. *Journal of Geophysical Research* 105: 6237–6254.

Lin WY (2000) Unstable groundwater supply after the big earthquake. *United Daily Newspaper*, Taiwan (in Chinese).

Linde AT and Sacks IS (2002) Slow earthquakes and great earthquakes along the Nankai trough. *Earth and Planetary Science Letters* 203: 265–275.

Linde AT, Sacks IS, Johnston MJS, Hill DP, and Bilham RG (1994) Increased pressure from rising bubbles as a mechanism for remotely triggered seismicity. *Nature* 371: 408–410.

Liu E, Vlatsos S, Li S-Y, Main IG, and Schoenberg M (2004) Modeling seismic wave propagation during fluid injection in a fractured network: Effects of pore fluid pressure on time-lapse seismic signatures. *Leading Edge* 23: 778–783.

Liu LB, Roeloffs E, and Zheng XY (1989) Seismically induced water level oscillations in the Wali well, Beijing, China. *Journal of Geophysical Research* 94: 9453–9462.

Lo T, Coyner KB, and Toksoz N (1986) Experimental determination of elastic anisotropy of Berea sandstone, Chicopee shale, and Chelmsford granite. *Geophysics* 51: 16471. http://dx.doi.org/10.1190/1.1442029.

Lockner DA and Beeler NM (2002) Rock failure and earthquakes. In: Lee WHK, Kanamori H, Jennings PC, and Kisslinger C (eds.) *International Handbook of Earthquake and Engineering Seismology*, pp. 505–537. San Diego, CA: Academic Press.

Ma KF, Lee CT, and Tsai YB (1999) The Chi-Chi, Taiwan earthquake: Large surface displacement on an inland thrust fault. *Eos, Transactions American Geophysical Union* 80: 605–611.

Maeda K and Yoshida A (1990) A probabilistic estimation of earthquake occurrence on the basis of the appearance times of multiple precursory phenomena. *Journal of Physics of the Earth* 38: 431–444.

Maltman AJ and Bolton A (2003) How sediments become mobilized. In: Van Rensberger P, et al. (eds.) *Subsurface Sediment Mobilization*, *Geological Society of London Special Publications*, vol. 216, pp. 9–20.

Manga M (2001) Origin of postseismic streamflow changes inferred from baseflow recession and magnitude-distance relations. *Geophysical Research Letters* 28: 2133–2136.

Manga M and Bonini M (2012) Large historical eruptions at subaerial mud volcanoes, Italy. *Natural Hazards and Earth System Sciences* 12: 3377–3386.

Manga M and Brodsky EE (2006) Seismic triggering of eruptions in the far field: Volcanoes and geysers. *Annual Review of Earth and Planetary Sciences* 34: 263–291.

Manga M, Brodsky EE, and Boone M (2003) Response of streamflow to multiple earthquakes and implications for the origin of postseismic discharge changes. *Geophysical Research Letters* 30. http://dx.doi.org/10.1029/2002GL016618.

Manga M, Brumm M, and Rudolph ML (2009) Earthquake triggering of mud volcanoes. *Marine and Petroleum Geology* 26: 1785–1798.

Manga M and Rowland JC (2009) Response of Alum Rock springs to the October 30, 2007 earthquake and implications for the origin of increased discharge after earthquakes. *Geofluids* 9: 237–250.

Manga M, Beresnev I, Brodsky EE, et al. (2012) Changes in permeability by transient stresses: Field observations, experiments and mechanisms. *Reviews of Geophysics* 50: RG2004. http://dx.doi.org/10.1029/2011RG000382.

Manning CE and Ingebritsen SE (1999) Permeability of the continental crust: Constraints from heat flow models and metamorphic systems. *Reviews of Geophysics* 37: 127–150.

Marone C, Carpenter BM, Rathbun AP, and Saffer DM (2010) Physical properties and mechanical behavior of the active San Andres Fault Zone: Insight from laboratory studies. *EOS Transactions American Geophysical Union*, abstract T52B04.

Mase CW and Smith L (1987) Effect of frictional heating on the thermal, hydrological, and mechanical response of a fault. *Journal of Geophysical Research* 92: 6249–6272.

Masson Y and Pride SR (2006) Poroelastic finite-difference modeling of seismic attenuation and dispersion due to mesoscopic-scale heterogeneity. *Journal of Geophysical Research* 112: B03204.

Matsumoto N (1992) Regression analysis for anomalous changes of ground water level due to earthquakes. *Geophysical Research Letters* 19: 1192–1196.

Matsumoto N and Roeloffs EA (2003) Hydrological response to earthquakes in the Haibara well, central Japan—II. Possible mechanism inferred from time-varying hydraulic properties. *Geophysical Journal International* 155: 899–913.

Mavko G, Mukerji T, and Dvorkin J (1998) *The Rock Physics Handbook: Tools for Seismic Data Analysis in Porous Media*. New York: Cambridge University Press.

Mazzini A, Svensen H, Akhmanov GG, et al. (2007) Triggering and dynamic evolution of the LUSI mud volcano, Indonesia. *Earth and Planetary Science Letters* 261: 375–388.

Mazzini A, Nermoen A, Krotkiewski M, Podladchikov Y, Planke S, and Svensen H (2009) Strike-slip faulting as a trigger mechanism for overpressure release through piercement structures. Implications for the Lusi mud volcano, Indonesia. *Marine and Petroleum Geology* 26: 1751–1765.

McEvilly T and Johnson L (1974) Stability of P and S velocities from central California quarry blasts. *Bulletin of the Seismological Society of America* 64: 343–353.

Mellors R, Kilb D, Aliyev A, Gasanov A, and Yetirmishli G (2007) Correlations between earthquakes and large mud volcano eruptions. *Journal of Geophysical Research* 112: B04304.

Micklethwaite S and Cox SF (2004) Fault-segment rupture, aftershock-zone fluid flow, and mineralization. *Geology* 32: 813–816.

Milkov AV (2000) Worldwide distribution of submarine mud volcanoes and associated gas hydrates. *Marine Geology* 167: 29–42.

Miller SA, Collettini C, Chiaraluce L, Cocco M, Barchi M, and Kaus BJP (2004) Aftershocks driven by a high-pressure CO_2 source at depth. *Nature* 427: 724–727.

Mizuno T (2003) The subsurface observation of fault-zone trapped waves: Applications to investigations of the deep structure of active faults. *Bulletin of the Earthquake Research Institute* 78: 91–106.

Mizuno T and Kuwahara Y (2008) Spatial variations in fault-zone structure along the Nojima fault, central Japan, as inferred from borehole observations of fault-zone trapped waves. *Bulletin of the Seismological Society of America* 98: 558–570.

Mogi K, Mochizuki H, and Kurokawa Y (1989) Temperature changes in an artesian spring at Usami in the Izu Peninsula (Japan) and their relation to earthquakes. *Tectonophysics* 159: 95–108.

Mohr CH, Montgomery DR, Huber A, Bronstert A, and Iroum A (2012) Streamflow response in small upland catchments in the Chilean coastal range to the MW 8.8 Maule earthquake on 27 February 2010. *Journal of Geophysical Research* 117: F02032. http://dx.doi.org/10.1029/2011JF002138.

Montgomery DR and Manga M (2003) Streamflow and water well responses to earthquakes. *Science* 300: 2047–2049.

Montgomery DR, Greenberg HM, and Smith DT (2003) Streamflow response to the Nisqually earthquake. *Earth and Planetary Science Letters* 209: 19–28.

Morrow C, Shi LQ, and Byerlee J (1984) Permeability of fault gouge under confining pressure and shear stress. *Journal of Geophysical Research* 89: 3193–3200. http://dx.doi.org/10.1029/JB089iB05p03193.

Mount VS and Suppe J (1987) State of stress near the San Andreas fault—Implications doe wrench tectonics. *Geology* 15: 1143–1146.

Muir-Wood R and King GCP (1993) Hydrological signatures of earthquake strain. *Journal of Geophysical Research* 98: 22035–22068.

National Research Council (1985) *Liquefaction of Soils During Earthquakes*, 240 pp. Washington, DC: National Academy Press.

Neuzil CE (2003) Hydromechanical coupling in geologic processes. *Hydrogeology Journal* 11: 41–83.

Nur A (1974) Matsushiro, Japan, earthquake swarm: Confirmation of the dilatancy-fluid diffusion model. *Geology* 2: 217–221.

Nur A and Booker JR (1972) Aftershocks caused by pore fluid flow? *Science* 175: 885–887.

Ohtani T, Tanaka H, Fujimoto K, Higuchi T, Tomida N, and Ito H (2001) Internal structure of the Nojima fault zone from Hirabayashi GSJ drill core. *The Island Arc* 10: 392–400.

Panahi BM (2005) Mud volcanism, geodynamics and seismicity of Azerbaijan and the Caspian Sea region. In: Martinelli G and Panahi B (eds.) *Mud Volcanoes, Geodynamics and Seismicity*, pp. 89–104. Dordrecht, The Netherlands: Springer.

Papadopoulos GA and Lefkopulos G (1993) Magnitude-distance relations for liquefaction in soil from earthquakes. *Bulletin of the Seismological Society of America* 83: 925–938.

Park SK (1997) Monitoring resistivity changes in Parkfield, California: 1988–1995. *Journal of Geophysical Research* 102: 24545–24559.

Park SK (2005) The agony and ecstasy of earthquake prediction (talk presented at U.S. Geological Survey, Menlo Park, CA).

Parotidis M and Shapiro SA (2004) A statistical model for the seismicity rate of fluid-injection-induced earthquakes. *Geophysical Research Letters* 31. http://dx.doi.org/10.1029/2004GL020421.

Plastino W, Povinec PP, De Luca G, et al. (2010) Uranium groundwater anomalies and L'Aquila earthquake, 6th April 2009 (Italy). *Journal of Environmental Radioactivity* 101: 45–50.

Pralle N, Külzer M, and Gudehus G (2003) Experimental evidence on the role of gas in sediment liquefaction and mud volcanism. In: Van Rensberger P, et al. (eds.) *Subsurface Sediment Mobilization*, *Geological Society of London Special Publications*, 216: 159–172.

Pride SR, Berryman JG, and Harris JM (2004) Seismic attenuation due to wave-induced flow. *Journal of Geophysical Research* 109: B01201. http://dx.doi.org/10.1029/2003JB002639.

Quigley MC, Bastin S, and Bdadley BA (2013) Recurrent liquefaction in Christchurch, New Zealand, during the Canterbury earthquake sequence. *Geology.* http://dx.doi.org/10.1130/G33944.1.

Quilty EG and Roeloffs EA (1997) Water level changes in response to the December 20, 1994 M4.7 earthquake near Parkfield, California. *Bulletin of the Seismological Society of America* 87: 1018–1040.

Raleigh CB, Healy JH, and Bredehoeft JD (1976) An experiment in earthquake control at Rangely, Colorado. *Science* 191: 1230–1237.

Rathbun AP, Song I, and Saffer D (2010) Permeability of the San Andreas fault zone at depth. *EOS Transactions American Geophysical Union*, abstract T41A2095.

Rice JR (1992) Fault stress state, pore pressure distributions, and the weakness of the san Andreas fault. In: Evans B and Wong T-F (eds.) *Fault Mechanics and Transport Properties of Rocks*, pp. 475–504. San Diego, CA: Academic Press.

Rice JR and Cleary MP (1976) Some basic stress diffusion solutions for fluid saturated elastic porous media with compressible constituents. *Reviews of Geophysics and Space Physics* 14: 227–241.

Rinehart JS (1972) Fluctuations in geyser activity caused by variations in earth tidal forces, barometric pressure, and tectonic stresses. *Journal of Geophysical Research* 77: 342–350.

Roeloffs EA (1996) Poroelastic techniques in the study of earthquake-related hydrologic phenomena. *Advances in Geophysics* 37: 135–195.

Roeloffs EA (1998) Persistent water level changes in a well near Parkfield, California, due to local and distant earthquakes. *Journal of Geophysical Research* 103: 869–889.

Roeloffs EA (2006) Evidence for aseismic deformation-rate changes prior to earthquakes. *Annual Review of Earth and Planetary Sciences* 34: 591–627.

Roeloffs EA and Quilty E (1997) Water level and strain changes preceding and following the August 4, 1985 Kettleman Hills, California, earthquake. *Pure and Applied Geophysics* 149: 21–60.

Roeloffs EA, Sneed M, Galloway DL, et al. (2003) Water-level changes induced by local and distant earthquakes at Long Valley caldera, California. *Journal of Volcanology and Geothermal Research* 127: 269–303.

Rojstaczer S, Ingebritsen SE, and Hayba DO (2005) Permeability of continental crust influenced by internal and external loading. *Geofluids* 8: 128–139.

Rojstaczer SA, Ingebritsen SE, and Hayba DO (2008) Permeability of continental crust influenced by internal and external forcing. *Geofluids* 8: 128–139. http://dx.doi.org/10.1111/j.1468-8123.2008.00211.x.

Rojstaczer S and Wolf S (1992) Permeability changes associated with large earthquakes: An example from Loma Prieta, California. *Geology* 20: 211–214.

Rojstaczer S, Wolf S, and Michel R (1995) Permeability enhancement in the shallow crust as a cause of earthquake-induced hydrological changes. *Nature* 373: 237–239.

Rojstaczer S, Galloway DL, Ingebritsen SE, and Rubin DM (2003) Variability in geyser eruptive timing and its causes: Yellowstone National Park. *Geophysical Research Letters* 30: Art. No. 1953.

Rudnicki JW, Yin J, and Roeloffs EA (1993) Analysis of water level changes induced by fault creep at Parkfield, California. *Journal of Geophysical Research* 98: 8143–8152.

Rudolph ML and Manga M (2010) Mud volcano response to the April 4, 2010 El Mayor–Cucapah earthquake. *Journal of Geophysical Research* 115: B12211. http://dx.doi.org/10.1029/2010JB007737.

Rudolph ML and Manga M (2012) Frequency dependence of mud volcano response to earthquakes. *Geophysical Research Letters* 39: L14303. http://dx.doi.org/10.1029/2012GL052383.

Saar MO and Manga M (2003) Seismicity induced by seasonal groundwater recharge at Mt. Hood, Oregon. *Earth and Planetary Science Letters* 214: 605–618.

Sato H (1978) Precursory land tilt prior to the Tonankai earthquake of 1944. In some precursors prior to recent great earthquakes along the Nankai trough. *Journal of Physics of the Earth* 25: s115–s121.

Sato H (1982) On the changes in the sea level at Tosashimizu before the Nankaido earthquake of 1946. *Journal of the Seismological Society of Japan* 35: 623–626.

Sato T, Sakai R, Furuya K, and Kodama T (2000) Coseismic spring flow changes associated with the 1995 Kobe earthquake. *Geophysical Research Letters* 27: 1219–1222.

Sato T, Matsumoto N, Kitagawa Y, et al. (2004) Changes in water level associated with the 2003 Tokachi-oki earthquake. *Earth, Planets and Space* 56: 395–400.

Savarensky EF (1968) On the prediction of earthquakes. *Tectonophysics* 6: 17–27.

Scholtz CH, Sykes LR, and Aggarwal YP (1973) Earthquake prediction—Physical basis. *Science* 181: 803–810.

Schuster RL and Murphy W (1996) Structural damage, ground failure, and hydrological effects of the magnitude (Mw) 5.9 Draney Peak, Idaho, earthquake of February 3, 1994. *Seismological Research Letters* 67: 20–29.

Seed H and Lee KL (1966) Liquefaction of saturated sands during cyclic loading. *Journal of the Soil Mechanics and Foundations Division* 92: 105–134.

Segall P (1989) Earthquakes triggered by fluid extraction. *Geology* 17: 942–946.

Segall P, Grasso JR, and Mossop A (1994) Poroelastic stressing and induced seismicity near the Lacq gas field, southwestern France. *Journal of Geophysical Research* 99: 15423–15438.

Semenov AM (1969) Variations in the travel-time of transverse and longitudinal waves before violent earthquakes. *Physics of the Solid Earth* 3: 245–248.

Shapiro SA, et al. (2006) Fluid induced seismicity guided by a continental fault: Injection experiment of 2004/2005 at the German Deep Drilling Site (KTB). *Geophysical Research Letters* 33: L01309. http://dx.doi.org/10.1029/2005GL024659.

Shi Z, Wang G, Wang C-Y, Manga M, and Liu C (2014) Comparison of hydrological responses to the Wenchuan and Lushan earthquakes. *Earth and Planetary Science Letters* 391: 193–200.

Sibson RH (1973) Interactions between temperature and pore-fluid pressure during earthquake faulting and a mechanism for partial or total stress relief. *Nature* 243: 66–68.

Sibson RH and Rowland JV (2003) Stress, fluid pressure and structural permeability in seismogenic crust, North Island, New Zealand. *Geophysical Journal International* 154: 584–594.

Sil S and Freymueller JT (2006) Well water level changes in Fairbanks, Alaska, due to the great Sumatra–Andaman earthquake. *Earth, Planets and Space* 58: 181–184.

Silver PG and Valette-Silver NJ (1992) Detection of hydrothermal precursors to large northern California earthquakes. *Science* 257: 1363–1368.

Simpson DW, Leith WS, and Scholz CH (1988) Two types of reservoir-induced seismicity. *Bulletin of the Seismological Society of America* 78: 2025–2050.

Sleep NH and Blanpied ML (1992) Creep, compaction and the weak rheology of major faults. *Nature* 359: 687–692.

Sorey ML and Clark MD (1981) Changes in the discharge characteristics of thermal springs and fumaroles in the Long Valley caldera, California, resulting from earthquakes on May 25–27, 1980. US Geological Survey Open-File Report 81-203.

Stein RS (1999) The role of stress transfer in earthquake occurrence. *Nature* 402: 605–609.

Steinberg GS, Merzhanov AG, and Steinberg AS (1982a) Geyser process: Its theory, modeling and field experiment. Part 1. Theory of the geyser process. *Modern Geology* 8: 67–70.

Steinberg GS, Merzhanov AG, and Steinberg AS (1982b) Geyser process: Its theory, modeling and field experiment. Part 3. On metastability of water in geysers. *Modern Geology* 8: 75–78.

Steinberg GS, Merzhanov AG, and Steinberg AS (1982c) Geyser process: Its theory, modeling and field experiment. Part 4. On seismic influence on geyser regime. *Modern Geology* 8: 79–86.

Stidham C, Antolik M, Dreger D, Larsen S, and Romanowicz B (1999) Three-dimensional structure influences on the strong-motion wavefield of the 1989 Loma Prieta earthquake. *Bulletin of the Seismological Society of America* 89: 1184–1202.

Su T-C, Chiang K-W, Lin S-J, Wang F-G, and Duann S-W (2000) Field reconnaissance and preliminary assessment of liquefaction in Yuan-Lin area. *Sino-Geotechnics* 77: 29–38.

Tadokoro K, Ando M, and Nishigami K (2000) Induced earthquakes accompanying the water injection experiment at the Nojima fault zone, Japan: Seismicity and its migration. *Journal of Geophysical Research* 105: 6089–6104.

Talwani P and Acree S (1985) Pore pressure diffusion and the mechanism of reservoir-induced seismicity. *Pure and Applied Geophysics* 122: 947–965.

Terzaghi K, Peck RB, and Mesri G (1996) *Soil Mechanics in Engineering Practice*, 3rd edn. New York: Wiley.

Tsunogai U, Maegawa K, Sato S, et al. (2012) Coseismic massive methane release from a submarine mud volcano. *Earth and Planetary Science Letters* 341–344: 79–85.

Thurber C, Roecker S, Ellsworth W, Chen Y, Lutter W, and Sessions R (1997) Two-dimensional seismic image of the San Andreas fault in the Northern Gabilan range, Central California: Evidence for fluids in the fault zone. *Geophysical Research Letters* 24: 1591–1594.

Tokunaga T (1999) Modeling of earthquake-induced hydrological changes and possible permeability enhancement due to 17 January 1995 Kobe earthquake, Japan. *Journal of Hydrology* 223: 221–229.

Townend J (1997) Subducting a sponge; minimum estimates of the fluid budget of the Hikurangi Margin accretionary prism. *Geological Society of New Zealand Newsletter* 112: 14–16.

Trique M, Richon P, Perrier F, Avouac JP, and Sabroux JC (1999) Radon emanation and electric potential variations associated with transient deformation near reservoir lakes. *Nature* 399: 137–141.

Tsunogai U and Wakita H (1995) Precursory chemical changes in ground water: Kobe earthquake, Japan. *Science* 269: 61–62.

Unsworth M, Bedrosian P, Eisel M, Egbert G, and Siripunvaraporn W (2000) Along strike variations in the electrical structure of the San Andreas Fault at Parkfield, California. *Geophysical Research Letters* 27: 3021–3024.

Wakita H (1975) Water wells as possible indicators of tectonic strain. *Science* 189: 553–555.

Wakita H (1996) Geochemical challenge to earthquake prediction. *Proceedings of the National Academy of Sciences* 93: 3781–3786.

Wakita H, Nakamura Y, and Sano Y (1988) Short-term and intermediate-term geochemical precursors. *Pure and Applied Geophysics* 126: 78–89.

Wang C-H, Wang CY, Kuo C-H, and Chen W-F (2005a) Some isotopic and hydrological changes associated with the 1999 Chi-Chi earthquake, Taiwan. *Island Arc* 14: 37–54.

Wang C-Y (1984) On the constitution of the San Andreas fault. *Journal of Geophysical Research* 89: 5858–5866.

Wang C-Y (2007) Liquefaction beyond the near field. *Seismological Research Letters* 78: 512–517.

Wang C-Y (2011) High pore pressure, or its absence, in the San Andreas fault. *Geology* 39: 1047–1050. http://dx.doi.org/10.1130/G32294.1.

Wang C-Y and Chia Y (2008) Mechanisms of water level changes during earthquakes: Near field versus intermediate field. *Geophysical Research Letters* 35: L12402. http://dx.doi.org/10.1029/2008GL034227.

Wang C-Y and Manga M (2010a) *Earthquakes and Water*. *Lecture Notes in Earth Sciences*, vol. 114. Springer.

Wang C-Y and Manga M (2010b) Hydrologic responses to earthquakes—A general metric. *Geofluids* 10: 206–216.

Wang C-Y, Wang C-H, and Kuo C-Y (2004a) Temporal change in groundwater level following the 1999 (Mw = 7.5) Chi-Chi earthquake, Taiwan. *Geofluids* 4: 210–220.

Wang C-Y, Wang C-H, and Manga M (2004b) Coseismic release of water from mountains: Evidence from the 1999 (Mw = 7.5) Chi-Chi, Taiwan, earthquake. *Geology* 32: 769–772.

Wang C-Y, Rui F, Yao Z, and Shi X (1986) Gravity anomaly and density structure of the San Andreas fault zone. *Pure and Applied Geophysics* 124: 127–140.

Wang C-Y, Cheng L-H, Chin C-V, and Yu S-B (2001) Coseismic hydrologic response of an alluvial fan to the 1999 Chi-Chi earthquake, Taiwan. *Geology* 29: 831–834.

Wang C-Y, Dreger DS, Wang C-H, Mayeri D, and Berryman JG (2003) Field relations among coseismic ground motion, water level change and liquefaction for the 1999 Chi-Chi (Mw = 7.5) earthquake, Taiwan. *Geophysical Research Letters* 17. http://dx.doi.org/10.1029/2003GL017601.

Wang C-Y, Dreger D, Manga D, and Wong A (2004c) Streamflow increase due to rupturing of hydrothermal reservoirs: Evidence from the 2003 San Simeon, California, earthquake. *Geophysical Research Letters* 31: L10502. http://dx.doi.org/10.1029/2004GL020124.

Wang C-Y, Manga M, Wang C-H, and Chen C-H (2012b) Transient change in groundwater temperature after earthquakes. *Geology* 40: 119–122.

Wang C-Y, Wang L-P, Manga M, Wang C-H, and Chen C-H (2013) Basin-scale transport of heat and fluid induced by earthquakes. *Geophysical Research Letters* 40. http://dx.doi.org/10.1002/grl.50738.

Wang C-Y, Wong A, Dreger D, and Manga M (2005c) Liquefaction limit during earthquakes and underground explosions—Implications on ground-motion attenuation. *Bulletin of the Seismological Society of America* 96: 355–363.

Wang R, Woith H, Milkereit C, and Zschau J (2004d) Modelling of hydrogeochemical anomalies induced by distant earthquakes. *Geophysical Journal International* 157: 717–726.

Wang HF (2000) *Theory of Linear Poroelasticity*, 287 pp. Princeton, NJ: Princeton University Press.

Wells DL and Coppersmith KJ (1994) New empirical relationships among magnitude, rupture length, rupture width, rupture area, and surface displacement. *Bulletin of the Seismological Society of America* 4: 964–1002.

Whitcomb JH, Garmany JD, and Anderson DL (1973) Earthquake prediction: Variation of seismic velocities before the San Fernando earthquake. *Science* 180: 632–635.

White DE (1967) Some principles of geyser activity, mainly from Steamboat Springs, Nevada. *American Journal of Science* 265: 644–684.

Wibberley C and Shimamoto T (2003) Internal structure and permeability of major strike-slip fault zones: The Median Tectonic Line in W. Mie Prefecture, S.W. Japan. *Journal of Structural Geology* 25: 59–78.

Wibberley CAJ and Shimamoto T (2005) Earthquake slip weakening and asperities explained by thermal pressurization. *Nature* 436: 689–692.

Wolf LW, Rowe CA, and Horner RB (1997) Periodic seismicity near Mt. Ogden on the Alaska-British Columbia border: A case for hydrologically-triggered earthquakes? *Bulletin of the Seismological Society of America* 87: 1473–1483.

Wong A and Wang CY (2007) Field relations between the spectral composition of ground motion and hydrological effects during the 1999 Chi-Chi (Taiwan) earthquake. *Journal of Geophysical Research* 112: B10305. http://dx.doi.org/10.1029/2006JB004516.

Wyss M and Booth DC (1997) The IASPEI procedure for the evaluation of earthquake precursors. *Geophysical Journal International* 131: 423–424.

Yan HR (2001) Water problems in the Yuenlin Mountains: Changes in groundwater after the Chi-Chi earthquake. *Chinese Daily,* Taiwan (in Chinese).

Youd TL (2003) Liquefaction mechanisms and induced ground failure. In: Lee WHK, Kanamori H, Jennings PC, and Kisslinger C (eds.) *International Handbook of Earthquake and Engineering Seismology, Part B*, pp. 1159–1173. San Diego, CA: Academic Press.

Zoback MD and Zinke JC (2002) Production-induced normal faulting in the Valhall and Ekofisk oil fields. *Pure and Applied Geophysics* 159: 403–420.

Zoback MD, Hickman S, and Ellsworth W (2010) Scientific drilling into the San Andreas fault zone—An overview of SAFOD's first five years. *Scientific Drilling* 11: 14–28.

Zoback MD, Zoback ML, Mount VS, et al. (1987) New evidence on the state of stress of the San Andreas fault system. *Science* 238: 1105–1111.